PROTEINS
STRUCTURE ■ FUNCTION ■ BIOINFORMATICS

Molecular mechanism of allosteric communication in the human PPARα-RXRα heterodimer

Tuomas Venäläinen,[1] Ferdinand Molnár,[2,3] Chris Oostenbrink,[4] Carsten Carlberg,[5,6] and Mikael Peräkylä[6]*

[1] Laboratory of Chemistry, Department of Biosciences, University of Kuopio, Kuopio FIN-70211, Finland
[2] Laboratoire de Biologie et de Génomic Structurale, Institut de Génétique et de Biologie Moléculaire et Celullaire, Illkirch 67400 Cedex, France
[3] Department of Pharmaceutics, University of Kuopio, Kuopio, FIN-70211, Finland
[4] Computational Medicinal Chemistry and Toxicology, Department of Chemistry and Pharmaceutical Sciences, Vrije Universiteit, Amsterdam, The Netherlands
[5] Life Sciences Research Unit, FSTC, University of Luxembourg, Luxembourg, L-1511, Finland
[6] Laboratory of Biochemistry, Department of Biosciences, University of Kuopio, Kuopio, FIN-70211, Finland

ABSTRACT

The peroxisome proliferator-activated receptor α (PPARα) is a nuclear receptor (NR) that forms a heterodimeric transcription factor complex with the retinoid X receptor α (RXRα). The phenomenon that the heterodimer can be activated by both PPARα and RXRα ligands, while both ligands have a synergistic effect on its activity suggests that there is an allosteric communication within the heterodimer. In this study, the molecular mechanism of this allosteric signaling was studied by molecular dynamics (MD) simulations and some of the residues involved in this communication were tested experimentally. Multiple MD simulations were done for the PPARα-RXRα heterodimer ligand-binding domains (LBDs) without ligands, with agonistic ligand bound to RXRα or PPARα, and ligand bound to both receptors. Fluctuation calculations and structural clustering analysis of the heterodimer MD simulations showed that ligand binding to RXRα decreases fluctuations of large parts of PPARα, most notably helices 3 and 4 at the coactivator binding site, which presumably stabilizes the coactivator binding to heterodimer complex. The dynamics of helix 8–9 loop and helix 10/11 located at the heterodimeric interface were affected by RXRα ligand binding, suggesting that these parts of the dimer are involved in allosteric communication. Experimental data complemented this view by showing that a large set of residues at the heterodimerization surface has a role in the communication. These results provided evidence that RXRα ligand binding-induced stabilization of PPARα coactivator binding site has a role in the permissive and synergistic activation of the PPARα-RXRα heterodimer.

Proteins 2010; 78:873–887.

Key words: molecular dynamics; nuclear receptors; protein-protein interactions; point mutations; activation.

INTRODUCTION

Allosteric communication of proteins plays a key role in regulation of many biological systems. Allosteric regulation is needed, for example, in mediating signals from outside of the cell into the cell by G-protein coupled receptors,[1] cooperative binding of oxygen molecules into hemoglobin[2] or the regulation of gene expression by nuclear receptors (NRs).[3] Common to these examples is that a small molecule binding to one part of the protein controls the biological activity in another part, which is located far away from the small molecule binding site or even in another protein. In this work, allosteric activation in a NR heterodimer of the peroxisome proliferator-activated receptor (PPAR) α and the retinoid X receptor (RXR) α is studied with molecular dynamics (MD) simulations and experimentally using reporter gene assays.

NRs form a superfamily of ligand-inducible transcription factors that regulate gene expression of a large variety of target genes. Natural NR ligands form a wide group of small lipophilic molecules including steroid hormones, fatty acids and xenobiotics, many of them important in cell regulation and metabolism.[4–6] This makes NRs interesting as drug targets. Binding of an agonist to the ligand-binding pocket (LBP) of a NR leads to a conformational change in the ligand-binding domain (LBD) leading to an interaction

Additional Supporting Information may be found in the online version of this article.
Grant sponsor: HPC-EUROPA Project; Grant number: RII3-CT-2003-506079; Grant sponsor: National Graduate School in Informational and Structural Biology.
*Correspondence to: Mikael Peräkylä, Laboratory of Biochemistry, Department of Biosciences, University of Kuopio, P.O. BOX 1627, Kuopio FIN-70211, Finland. E-mail: mikael.perakyla@uku.fi.
Received 18 June 2009; Revised 26 August 2009; Accepted 2 September 2009
Published online 17 September 2009 in Wiley InterScience (www.interscience.wiley.com). DOI: 10.1002/prot.22613

with coactivator proteins.[7] The largest conformational change occurs in the C–terminal helix 12, which acts as a molecular switch allowing either coactivator or corepressor protein binding. Agonist binding favors a conformation, in which helix 12 is docked against the helices 3 and 11 forming one side of the activation function 2 (AF-2) surface and facilitating coactivator binding.[8] Antagonists prevent binding of helix 12 against the core of the LBD and formation of the coactivator binding surface.[7] Without an agonist or with an antagonist, many of the NRs bind a corepressor protein and their target genes are silenced.[4]

The outcome of the NR action depends on the coregulator proteins bound. Often there is a balance between coactivator and corepressor proteins, which is controlled by helix 12. The conformation of helix 12 in turn is modulated by ligand binding. Thus, the final outcome depends on the relative concentrations of the coregulatory proteins, ligand binding, ligands' properties, and the nature of the receptor itself. Many of the NRs like retinoic acid receptor α (RARα), vitamin D receptor (VDR), thyroid hormone receptor (TR), and steroid hormone receptors are not active without an agonist, whereas others, such as PPARs and constitutive androstane receptor (CAR) have significant constitutive activity.[9,10]

Although the conformation of helix 12 is the main determinant of NR LBD controlled activation and repression, other more subtle structural and dynamical factors have been observed. Bruning *et al.* showed by the amide H/D exchange (HDX) method that binding of intermediate and partial agonists lead to considerably lower stabilization of PPARγ helix 12, but unexpectedly, they stabilized other parts of the LBD, mainly the β-sheet area and helix 3.[11] It was also shown that stabilization of helices 3 and 11 is not sufficient to stabilize helix 12. Similar observations were made by computer simulations on the glucocorticoid receptor (GR) and its mutants. In these MD simulations, an increased biological activity was found to correlate with reduced fluctuations of helices 3, 4, and 5.[12] MD simulations have also suggested that ligand binding modifies LRH-1-cofactor interactions without causing overall changes in to protein structure.[13] In addition, by a new class of PPARα/γ agonists it could be shown that direct stabilization of helix 12 by ligand binding is not necessary for PPAR agonism.[14,15] These ligands were shown by X-ray crystallography to adopt a novel binding mode lacking contacts with helices 11 or 12. Taken together, these results suggest that a helix 12 independent mechanism contributing to NR activation exists.

Many NRs function as heterodimers with RXR.[4,7] Heterodimer formation is required for efficient contact to DNA binding sites, so-called response elements, in primary NR target genes. On the basis of the heterodimer's response to ligands, NRs can be classified to be permissive or nonpermissive.[3] Permissive receptors can be activated also with RXR ligand and they give full response when ligands are bound to both receptors of the heterodimer, whereas nonpermissive receptors do not respond to RXR ligand, but give a full response with their own ligand.[3] Conditionally permissive receptors display synergy, or increased activity with two ligands, but cannot be activated with RXR ligand alone.[16]

To better understand the mechanism of permissivity, its dynamic nature and synergistic activation of NRs in general at the atomic level, we studied the PPARα-RXRα heterodimer with different combinations of ligands using MD simulations. PPARα was chosen for this study because of its key role in lipid metabolism and its highest constitutive activity among the three PPAR subtypes.[17] From the MD simulations, we have identified residues involved in the communication between the two monomers in the PPARα-RXRα complex and our model has been investigated experimentally using reporter gene assays. This study provided new information of ligand-induced intermonomeric allosteric communication in the PPARα-RXRα heterodimer, which may be applied to the other NR heterodimers with permissive activation profile.

METHODS

Constructing the simulations systems

Because there were no crystal structures available for the PPARα-RXRα heterodimer, a PPARγ-RXRα heterodimer structure was used as template. In this original PPARγ-RXRα structure (Protein Data Bank (PDB) code 1K74[18]) 9-cis retinoic acid (9cRA) is bound to the RXRα, GW409544 (GW) is bound to the PPARγ, and two coactivator peptides are bound to the complex. From the template, PPARγ was replaced with the PPARα structure (PDB code 1K7L[18]). For the simulations, the coactivator peptides were removed, because they were expected to stabilize the receptor into the active conformation and to mask the effects of the ligands.

The resulting PPARα-RXRα heterodimer contained 499 amino acid residues. Crystallographic water molecules from the PPARγ-RXRα heterodimer were kept, when they did not overlap with PPARα residues. Side chains of PPARα residues at the heterodimer interface were rotated to the same conformations, as observed in the PPARγ-RXRα heterodimer. This could be determined unambiguously, because the residues of the heterodimer interface of the two PPAR subtypes are highly conserved. Four PPARα-RXRα MD simulation systems were constructed: (1) apo heterodimer: the unliganded LBD heterodimer, (2) 9cRA heterodimer: 9cRA bound to the RXRα LBD with PPARα unliganded, (3) GW heterodimer: GW bound to the PPARα LBD with RXRα unliganded, and (4) 9cRA + GW heterodimer: ligands bound to both RXRα and PPARα LBDs. The dimeric complexes were placed in a periodic box of 7.3 × 9.9 × 8.3 nm containing ∼17,000 SPC water molecules. The

net charge of the system (−12 with two ligands) was neutralized with randomly positioned Na^+-ions.

MD simulations

All the simulations were performed using the GROMACS program[19] with the GROMOS 45a3 force field.[20] The missing parameters for the ligands were derived by analogy to the amino acid parameters in the GROMOS force field (Supporting Information Tables S1–S10). The LINCS[21] method was used to constrain all the bond lengths of the protein and the ligands and the SETTLE algorithm[22] was used to constrain all the bond lengths and angles of the water molecules. The time step for the leap-frog algorithm was set to 2 fs. A twin range cut-off was used for nonbonded interactions updating the neighbor list within the short range cut-off radius at 8 Å every 10 steps, at which times interactions in the intermediate range (14 Å) were also calculated. A reaction field contribution[23] with a relative dielectric permittivity of 62.0[24] was added to the electrostatic energies and forces to account for long-range interactions outside the cut-off sphere. During the MD simulations rotation and translation of the protein was removed every 10 steps.

Initial velocities were sampled randomly from a Maxwell-Bolzmann distribution at 100 K. The water molecules of the simulation systems were first heated at constant volume from 100 to 300 K in 120 ps with position restraints on the protein heavy atoms. The protein was then equilibrated at 300 K at constant pressure conditions for 250 ps while slowly releasing protein restraints. Finally, the systems were equilibrated for 300 ps at constant pressure. Temperature and pressure were controlled with the Berendsen weak coupling algorithm[25] with coupling constants of 0.1 and 0.5 ps, respectively. After that, production simulations of 2 ns were started. Ten parallel MD simulations for each simulation system were started after the equilibration phase by randomly assigning new starting velocities. Coordinates were stored every 0.1 ps. Average structures of the last 500 ps of the production trajectories were used in structural analysis and the last 1 ns was used for the fluctuation and structural clustering calculations. Other sampling times were also tested with no change in the conclusions.

To validate our methods, ten parallel simulations were performed for the PPARα and RXRα monomers using the same computational protocols as in the heterodimer simulations. The results are presented in the Supporting Information.

Compounds

The mouse CAR agonist TCPOBOP was kindly provided by Dr. P. Honkakoski (University of Kuopio). $1\alpha,25(OH)_2D_3$ and the PPARδ agonist L763483 were a gift from Drs. L. Binderup and M. W. Madsen (Leo Pharma, Ballerup, Denmark). The 9cRA, methoprene acid, GW7647 and the 25-OH cholesterol were obtained from Biomol (Copenhagen, Denmark). 9cRA and $1\alpha,25(OH)_2D_3$ was dissolved in ethanol and 2-propanol, respectively, whereas the other compounds were dissolved in dimethyl sulfoxide (Me_2SO). Further dilutions were made in Me_2SO.

Protein expression vectors

Full-length cDNAs for human PPARα,[26] human RXRα,[27] human VDR,[28] human LXRβ,[29] and human RARα[30] were subcloned into the T7/SV40 promoter-driven pSG5 expression vector (Stratagene), mouse CAR[31] into the CMV promoter-driven vector pCMX and that for human PPARδ[32] into the CMV promoter-driven vector pcDNA3 (Invitrogen). The point mutants of PPARα and RXRα were generated by using the QuickChange site-directed mutagenesis kit (Stratagene) according to the manufacturer's instructions. All mutations were confirmed by sequencing.

Reporter gene constructs

Four copies of the human *CPTI* gene DR1-type RE (core sequence GTAGGGAAAAGGTCA),[33] four copies of the rat *ANF* gene DR3-type RE (core sequence AGAGGT CATGAAGGACA),[34] one copy of the PBREM element from mouse *CYP2B10* gene promoter (core sequence GAGTGTCAGGCAAGTTGATGGTGCACTGTGCCAAGG TCAGGAAAGTACAGA),[35] four copies of the human *iNOS* gene promoter DR4-type RE (core sequence GTGGTTCATGCCGGTTCA)[36] and two copies of the consensus DR5(T/T)-type RE (AGAGTTCACCGAAAGT TCA) were individually fused with the thymidine kinase (tk) minimal promoter driving the firefly luciferase reporter gene.

Transient transfection and luciferase reporter assays

HEK293 human embryonic kidney cells were seeded into 6-well plates (200,000 cells/well) and grown overnight in phenol red-free Dulbecco's modified Eagle's medium (DMEM) supplemented with 5% charcoal-stripped fetal bovine serum. Plasmid DNA containing liposomes were formed by incubating 1 μg of an expression vector for wt and mutant PPARα and/or RXRα and 1 μg of reporter plasmid bearing four copies of the human CPTI DR1-type RE with 10 μg of DOTAP (Roth, Karlsruhe, Germany) for 15 min at room temperature in a total volume of 100 μL. After dilution with 900 μL of phenol red-free DMEM, the liposomes were added to the cells. Phenol red-free DMEM supplemented with 500 μL of 15% charcoal-stripped fetal bovine serum was added 4 h after transfection. At this time, 10 n*M* 9cRA, 100 n*M* of PPARα selective agonist GW7647, the combination of

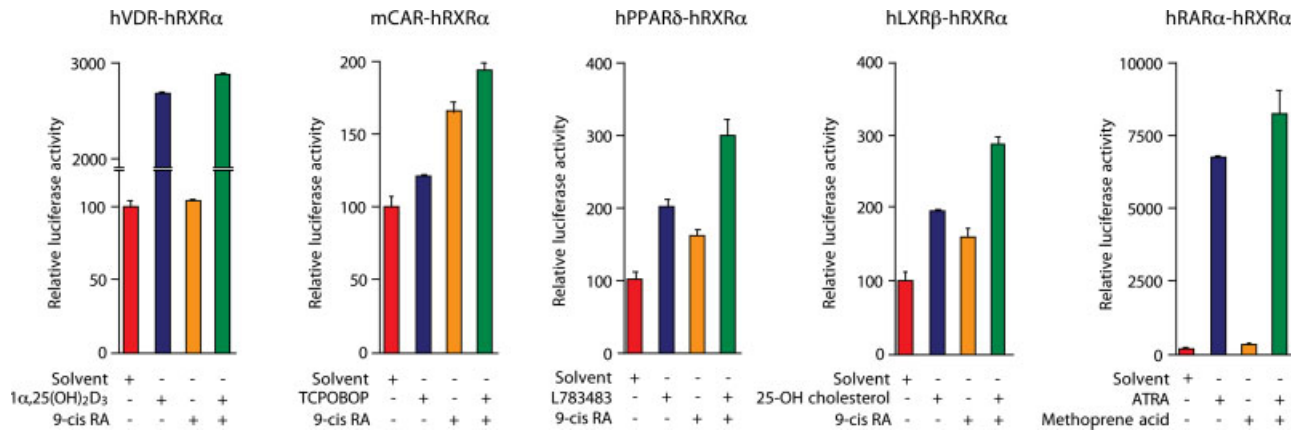

Figure 1

Differential response of RXR heterodimers to ligands. From left: Nonpermissive heterodimer pSG5-hVDR on the *tk*-[rANF DR3 VDRE]$_4$-luc reporter plasmid in HEK293 cells in the presence of endogenous RXR, treated with 100 n*M* 9cRA RXR agonist and 100 n*M* 1α,25(OH)$_2$D$_3$. Permissive heterodimers: Activation of *tk*-PBREM-luc reporter by pCMX-mCAR in HEK293 cells and by treatment with 100 n*M* 9cRA and the 1 μ*M* mouse CAR agonist TCPOBOP, pcDNA3-hPPARδ on the tk-[hmCPTI DR1 PPRE]$_4$-luc reporter plasmid in HaCaT cells in the presence of endogenous RXR, treated with 100 n*M* 9cRA RXR agonist and 100 n*M* L783483, tk-[hiNOS DR4 LXRE]$_4$-luc reporter in the presence of pSG5-hLXRβ in HEK293 cells and by treatment 100 n*M* 9cRA and 10 μ*M* LXR agonist 25-OH cholesterol. Conditionally permissive heterodimer: Activation of a tk-[consensus DR5 T/T RARE]$_2$-luc reporter by pSG5-hRARα in HaCaT cells and by treatment with 1 μ*M* methoprene acid (RXRα specific agonist with no activity on RAR) and 10 n*M* RAR agonist ATRA. The adequate ligand conditions are indicated in color bars: Apo (red); 9cRA (orange); RXR partner's ligand (blue); 9cRA + RXR partner's ligand (green).

9cRA and GW7647 or solvent was also added. The cells were lysed 16 h after the onset of stimulation using the reporter gene lysis buffer (Roche Diagnostics), and the constant light signal luciferase reporter gene assay was performed as recommended by the supplier (Canberra-Packard, Groningen, The Netherlands). The luciferase activities were normalized with respect to protein concentration. A two-tailed, paired Student's *t*-test was performed, and *P* values were calculated in reference to the solvent control ($^*P < 0.05$; $^{**}P < 0.01$; $^{***}P < 0.001$).

RESULTS

Differential response of RXR heterodimers to ligands

PPARs belong to the permissive group of NRs since in cell-based assay the PPAR-RXR heterodimer is activated also when only 9cRA is present, whereas the nonpermissive VDR-RXR complex shows no extra activation with 9cRA compared to its apo state. Conditionally permissive heterodimers, such as RAR-RXR, show very week activation when RXR specific ligand, for example, methoprene acid, is bound to the heterodimer (Fig. 1).

PPARα-RXRα LBD heterodimer stability in the simulations

To investigate the stability of the simulations, the atom-positional root-mean-square deviation (RMSD) of the Cα atoms relative to the crystal structure (Supporting Information Fig. S4) were calculated. The RMSD values in all heterodimer simulations were clearly lower (by ~0.5 Å) than those in the monomer simulations (Supporting Information Figs. S2 and S3) being mostly <2Å. This indicates that the MD simulations were stable and that heterodimer formation stabilizes the LBDs. Heterodimer simulations with 9cRA bound to RXRα seem to stay closer to the starting structure than the simulations without 9cRA.

Ligand binding restricts the movements of the heterodimer

To further investigate the ligand effects on the heterodimer flexibility, average structures of the last 500 ps of the parallel MD simulation were compared. The 10 parallel average structures of each ligand condition were superimposed using the Cα atoms (Fig. 2). In overall, the apo heterodimer showed higher differences between the average structures compared to conditions where ligands were present [Fig. 2(A)]. Helices 6 and 7 of the RXRα have the highest flexibility in the apo and GW bound heterodimers and the lowest when 9cRA and both 9cRA and GW are present. Interestingly, PPARα was more rigid in all conditions compared to RXRα.

The tilt angle of helices 10–11 (K449 /Cα(PPARα)-D466/Cα(PPARα)- F438/Cα(RXRα)) in the heterodimer is lower when ligands are bound. Binding of 9cRA has a larger effect on the angle than GW binding [Fig. 2(A)]. However, there is no significant change in the dihedral angle between the residues K449/Cα(PPARα)-D466/

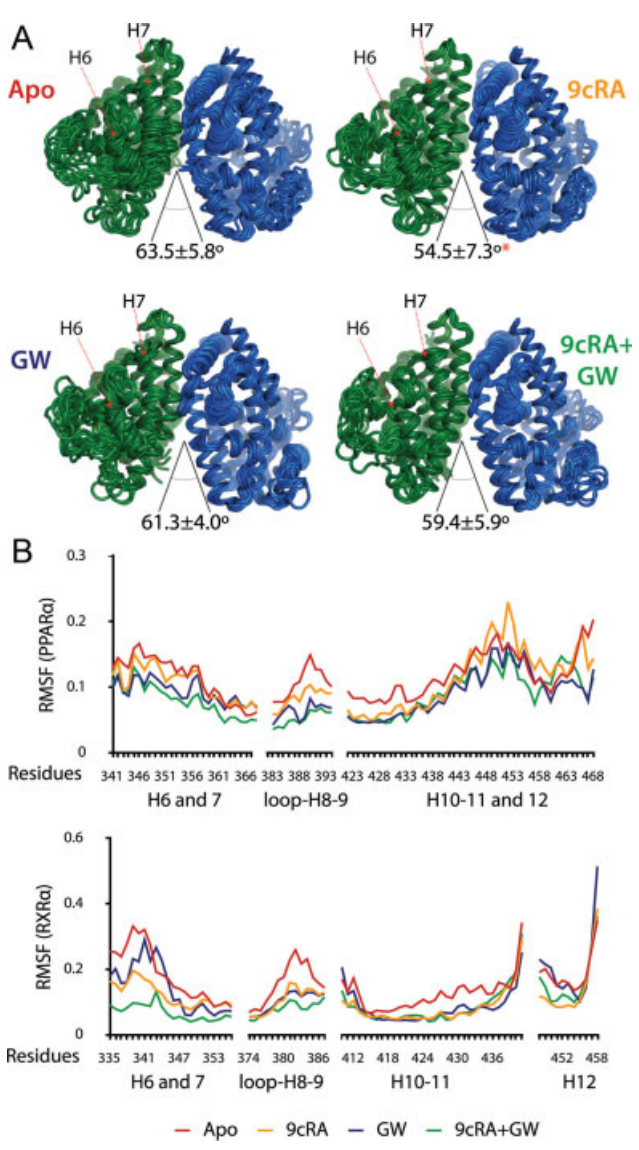

Figure 2

Ligand binding restricts the movements of the heterodimer. The 10 superimposed average structures for every ligand condition from the last 500 ps of the MD simulations are visualized in tube representation. (**A**) Below the structures the angle between the helices 10–11 of PPARα and RXRα is indicated and the helices 6 and 7 are highlighted with red arrows. The graphical representation of the structural differences (RMSF data) of the heterodimeric complex for every residue at the heterodimerization interface is shown in detail. (**B**) The different ligand conditions are displayed in colored lines: Apo (red); 9cRA (orange); GW (blue); 9cRA + GW (green).

Cα(PPARα)-L430/Cα(RXRα)- F438/Cα(RXRα) indicating that the tilting takes place only about one axis. The PPARα's helix 12 (the distance between P458/Cα and Y468/Cα) was significantly shorter in the presence of GW (17.22 ± 1.13 Å*) compared to apo protein (18.27 ± 0.97 Å). This is most likely due to stabilization of PPARα's C-terminus by direct interaction with helix 10/11 of RXRα in the apo heterodimer, whereas in the presence of GW the inter-molecular stabilization is partly replaced by intra-molecular interactions.

To obtain a quantitative measure of the structural differences, atom-positional root-mean-square fluctuations (RMSFs) around the average positions of Cα atoms were measured for the 10 parallel average structures [Fig. 2(B)]. The RMSF values of the helices 7, 10–12 and the helix 8,9 loop at the heterodimer interface show that differences between the parallel structures are highest in the apo heterodimer, and lowest in the GW + 9cRA heterodimer. It is also seen, that binding of a ligand to one monomer leads to more regular behavior of the other monomer.

In conclusion, binding of ligands leads to more regular behavior of the heterodimer, which is seen in the smaller differences between the average structures of the parallel MD simulations. Narrowing of the tilt angle of the helices 10/11 is likely to be connected with the ligand binding –induced changes in the behavior of the heterodimer.

Ligand binding increases packing at the heterodimerization surface

Analyses of the average structures of the last 500 ps of the simulations show that ligand binding pushed helices 7 and 11 of PPARα and RXRα closer to the partner protein, which decreased their separation across the heterodimer interface. For example, the distance between the two helix 11 residues K431 (RXRα) and T438 (PPARα) was on average 1.0 Å shorter in the 9cRA simulations than in the apo simulations. Another helix 11–helix 11 distance, E434 (RXRα)- Q442 (PPARα), was 1.8 Å shorter in the 9cRA simulations than in the apo simulations, and 0.9 Å shorter in the GW simulations than in the apo simulations. This was also seen in the angle of the helices 10/11 [Fig. 2(A)].

To further analyze the structural change, the dimerization surface area of each PPARα-RXRα system was calculated. The solvent accessible surface area of PPARα-RXRα heterodimer was calculated for every 1 ps and subtracted from the sum of surface areas of PPARα and RXRα calculated separately. The average surface areas buried upon heterodimer formation calculated from 10 parallel MD simulations were 1740 ± 130 Å^2, 1700 ± 90 Å^2, 1750 ± 70 Å^2, and 1780 ± 50 Å^2 in the apo-, 9cRA-, GW- and GW + 9cRA systems, respectively. According to the *t*-test, only when 9cRA simulations were compared to GW + 9cRA simulations the dimerization areas were found to be different at 95% confidence level. These results suggest that ligand binding induced conformational changes in the helices 7 and 11 may increase the dimerization surface and thus stabilize the heterodimer partner. However, this increase is small and could not be seen in the case of 9cRA binding, even though the change in the helix 11-helix 11 angle was

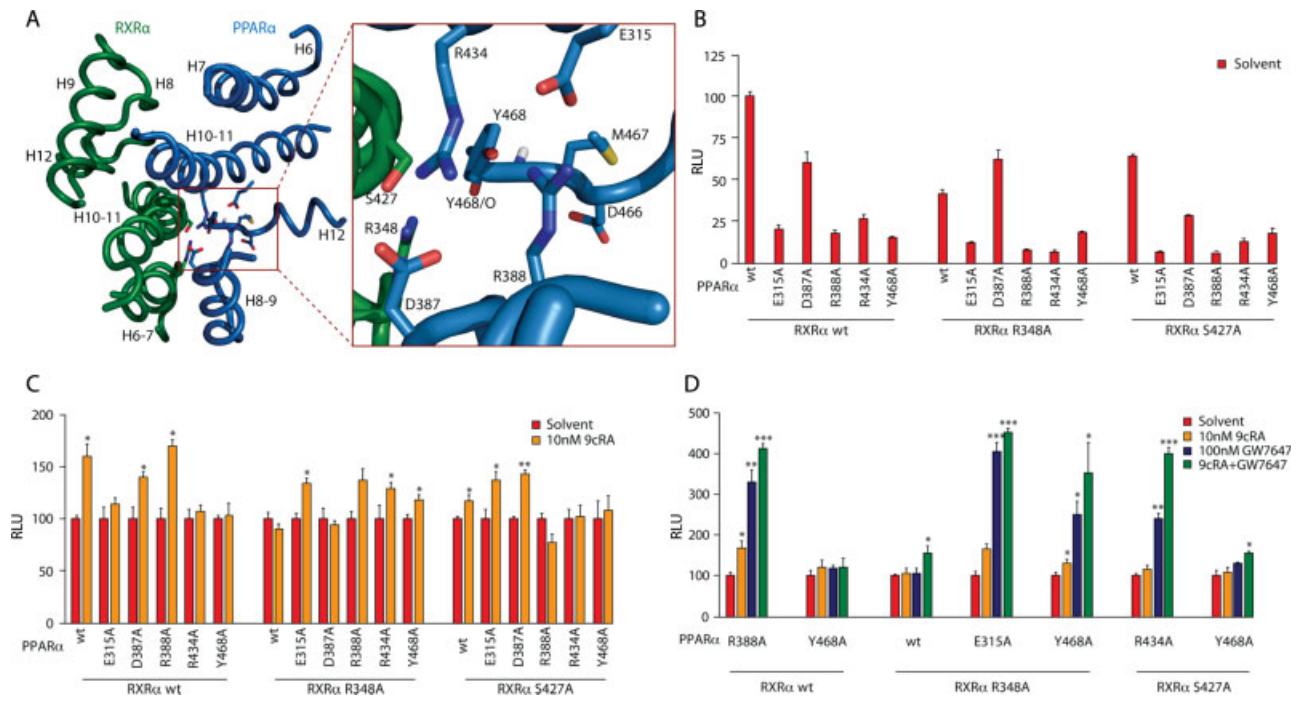

Figure 3

Allosteric communication at the heterodimerization interface. The heterodimerization interface of PPARα (in green)-RXRα (in blue) is shown. Location of amino acid residues R348 and S427 in RXRα, and E315, D387, R388, R434, and Y468 in PPARα mutated in this work are shown in detail. (**A**) Basal and ligand-induced activities of the wild type (wt) and mutated PPARα-RXRα heterodimers were measured using extracts from HEK293 cells that were transiently transfected with a reporter construct containing four copies of the human *CPTI* DR1-type RE and expression vectors for wt and mutant PPARα and/or RXRα. Cells were treated for 16 h with solvent (**B**), 10 n*M* 9cRA (**C**), 100 n*M* of PPARα selective agonist GW7647 or with the combination of 9cRA and GW7647 (**D**). The data were normalized to the activity of the wt heterodimer (B) or to the solvent treated condition (C and D). Columns represent the mean of at least three experiments, and bars indicate S.D. A two-tailed, paired Student's t test was performed, and p values were calculated in reference to the solvent control (*, $P < 0.05$, **, $P < 0.01$, ***, $P < 0.001$). Red color column bars indicate basal activities in apo state (B, C, D), the orange column show the ligand inducibilities when 9cRA was present (C, D) and the blue and green columns bars indicate the ligand conditions when GW7647 and 9cRA + GW7647 were present, respectively.

largest in that case [Fig. 2(A)]. On the basis of the standard deviations of the average surface areas, the apo systems showed the most irregular behavior of the MD simulations.

In summary, the MD simulations showed that ligand binding leads to changes in the PPARα-RXRα LBD heterodimer, which bring helices 11 of the two receptors closer to each other. The result of this conformational change is an increase in the intensity of packing at the dimerization surface and possibly slightly increased dimerization surface area.

Direct PPARα helix 12 stabilization by RXRα helices 7 and 11

The C-terminus of apo PPARα's helix 12 was seen to adopt a position in which it is closer to RXRα than in a liganded PPARα. On the other hand, binding of 9cRA to RXRα relocated helices 7 and 11 of RXRα towards helix 12 of PPARα, which stabilized its position by a hydrogen bond between K431 of RXRα and R348 of PPARα. This mechanism may explain at least part of the RXRα ligand-induced activation of PPARα, as it has been suggested by Gampe *et al.* on the basis of crystal structures of the PPARγ-RXRα LBD heterodimer.[37]

Allosteric communication at the heterodimerization interface

The heterodimerization interface of PPARα-RXRα consists of the helices H6-7, H8-9, H10/11, and helix 12 [Fig. 3(A)]. The information exchange between the monomers takes place through this interface and it can be disturbed by mutating the residues in these parts of the proteins.

The effect of an alanine mutation depends on the relative importance of the mutated residue, the nature of the interaction of that residue with other parts of the complex and resulting changes on the protein structure. Ideally, alanine mutation on the heterodimerization interface reveals the relative importance of the mutated residue on the communication between the monomers. However, the resulting change in the activation profile of

Table I
Interactions Between Residues at the Heterodimerization Interface

Interaction (PPARα-RXRα)	Ligand conditions in the MD simulations			
	Apo (%)	9cRA (%)	GW (%)	9cRA + GW (%)
H7 H8-9 K364-D379	30	30 (+10)	10 (+30)	60 (+30)
H8-9 H7 G386/O-K356	0	0	20	0
H8-9 H7 D387-R348	10	0	10	0
H8-9 H7 P389/NH-E352	0	0	10	0
H9 H7 E398-K356	20	10	0	40 (+ 20)
H9 H9-10 R409-E401	10	0	0	0
H9 H10 E402-K417	10	0	0	0
H10 H9 K425/O-E394	(+50)	(+40)	(+90)	60 (+10)
H10 H9 Q428-R393	0	0	20	10
H10 H9 Q428-Y397	0	0	10	0
H10 H10 A431/O-R426	0	10	20	0
H10 H10 D432-R426	20	60	40	20
H10 H10 R434-P423/O	0	40	80	80
H10 H10 R434-S427	60	60	90	90
H10 H7 R434-E352	0	10	0	0
H11 H10 Q435-R426	40	70	70	80 (+20)
H11 H10-11 Q442-E434	0	10	0	0
H12 H7 D466/O-R348	0	10	0	0
H12 H7 M467/O-R348	0	30	0	0
H12 H10 Y468-S427	0	10	0	0
H12 H7 Y468/O-R348	40	10 (+30)	0	10
H12 H10 Y468/O-K431	10	50 (+20)	20 (+10)	10 (+10)

The table lists all the hydrogen bond capable interaction (distance <3.5 Å) of the residues located at the heterodimerization interface. The values (in %) represent the occurrence of the interactions in 10 independent MD simulations, and the values in brackets express the additional possibilities where the distance of the hydrogen bond is between 3. 5 and 4.0 Å.

the complex can be weaker, if the mutation is compensated by other contacts, or stronger, if mutation of a large residue into alanine leads to structural changes that modify also other contacts between the monomers. We expect an alanine mutation on a hydrophobic residue to be more easily compensated than a mutation of a hydrogen bond forming residue, because the strength of a hydrogen bond depends largely on the angle and the distance between the donor and the acceptor. The resulting effect of the mutation of a hydrogen bond forming residue is expected to be stronger and to tell more about the importance of that residue on the allosteric communication, although the compensating hydrogen bonds with back bone or with other residues or other structural changes cannot be avoided.

The average structures of the MD simulations were examined to identify candidate residues, which are able to form hydrogen bonds at the heterodimerization interface (Table I). In the table, the percentage of occurrence of a hydrogen bond is indicated in all the four ligand conditions. Some interactions such as R434 (PPARα)- P423/C=O (RXRα) or R434 (PPARα)- S427 (RXRα) are seen under most of the conditions indicating the significance of these residues in the intermonomeric interaction. The interactions, which are formed occasionally (indicated with smaller % value in Table I) may compensate a mutation.

To examine the information flow through the dimerization surface, the following amino acid residues were substituted with alanine residue: E315, D378, R388, R434, and Y468 found in human PPARα and R348 and S427 in RXRα [Fig. 3(A)]. These residues are located at the heterodimerization interface in H6-7 and H10-11 of RXRα and H8-9, H10-11 and H12 of PPARα. For instance, the residue R348 (RXRα) in the apo state is able to make contacts with four different residues in PPARα (D387, D466/C=O, Y468/Oterm1, and M467/C=O) showing some alternative options for the communication. We also suspect that this residue may be involved in the intra-helical stabilization of the RXRα H10/11. The drop of the basal activity of the heterodimer to 41% compared to the wild-type receptor is the combined effect of all these functions connected to R348 (RXRα) [Fig. 3(B)]. The PPARα residues E315, D387, R388, and R434 are placed in the close proximity to the heterodimerization interface and also stabilize directly the PPARα helix 12 through the contact with Y468 [Fig. 3(A)]. This interaction is more visible in the apo state of the heterodimer, when the high basal activity is mediated also through this stabilization. The critical role of these residues is highlighted by a marked drop of the basal activities when mutated to alanine [Fig. 3(B)]. Although a PPARα mutant in combination with a RXRα mutant usually results in an additional decrease in the basal activity [Fig. 3(B)], the activity of PPARα Y468A mutant is not affected further when combined with R348A or S427A RXRα mutants. A particularly interesting profile can be seen for the mutation D387A: with wild-type RXRα the basal activity is decreased to 59% and in combination with R348A (RXRα) it is 61.5% compared to the wild-type heterodimer.However, in combination with S427A the basal activity is as low as 28% due to the indirect effect of the D387 (PPARα)- R434 (PPARα)- S427 (RXRα) interaction, where the R434 (PPARα)- S427 (RXRα) contact is also compromised and the additional hydrogen bond between R434 (PPARα)- P423/C=O cannot rescue the abolished interaction. This results in a condition, where R434 (PPARα) cannot adopt its correct conformation for the effective allosteric communication [Figs. 3(A,B)].

Next, the combinations of all mutants were tested in the presence of 10 n*M* 9cRA [Fig. 3(C)]. Unsaturated concentration of 9cRA was used in order to see subtle differences between the mutant profiles. Although the basal activities of the mutants showed high differences [Fig. 3(B)], the 9cRA induction was normalized to the solvent for comparison of the levels of induction by 9cRA. The obtained results show induction profiles varying from almost wild-type level (PPARα mutations D387A and R388A) to total loss of induction (for example PPARα mutations E3135A, R434A, and Y468A). Introducing a second mutation can result in decrease [R348A (RXRα) combined with D387A or R388A of PPARα, S427A

(RXRα) combined with R338A of PPARα] or increase [R348A (RXRα) combined with E315A, R434A or Y468A of PPARα, S427A (RXRα) combined with E315 of PPARα] of the induction level compared to the single mutation. The results show that balanced cowork of multiple residues on the heterodimerization interface is needed for successful communication between the monomers.

Finally some of the PPARα-RXRα mutant combinations were chosen to test the full panel of ligand conditions. The concentration of 9cRA was 10 n*M* and the concentration of available PPARα selective agonist GW7647 was 100 n*M*. The reasons for choosing this compound were that GW409544 is commercially not available and both ligands are strong PPARα selective agonists. In addition, the choice of this agonist seems to be in agreement with the recently published PPARγ-RXRα crystal structures, which showed no differences between the domain organization of the full length heterodimer when bound to different type of ligands.[38] It must be also noted that the MD simulations were done with GW409544, since PPARα has been cocrystallized with this compound and the docking of GW7647 could have led to errors in the initial structure used for MD simulations. The different profiles obtained with full panel of ligand combinations largely vary from phenotypes resembling the wild-type heterodimer [R388A (PPARα)- wt (RXRα), E315A (PPARα)- R348A (RXRα), and Y468A (PPARα)- R348A (RXRα)], to profiles where only 9cRA signaling was affected [R434A (PPARα)- S427A (RXRα)]. Also profiles where some of the communication was selectively diminished [wt (PPARα)- R348A (RXRα) and Y468A (PPARα)- S427A (RXRα)] and profiles where all the communication was blocked [Y468A (PPARα)- wt (RXRα)] [Fig. 3(D)] were observed.

Two main conclusions can be drawn from this mutation data: (1) All the residues mutated in this study, also those located far away from the helix 12, have a role in the permissive activation of the PPARα-RXRα heterodimer. (2) The effects of the mutations are not additive: combining two point mutations can reverse the effects of the single point mutations alone. In case of PPARα agonist and when 9cRA and GW7647 are combined the situation is even more complex. It has been shown that under these condition PPARα agonists contribute largely to the stabilization of helix 12 activating the heterodimer [Fig. 3(D)].[10]

9cRA binding to RXRα increases the stability at the coactivator binding site of PPARα

RMSFs around the average positions of Cα atoms were measured from the last 1 ns of the 2 ns MD simulations. For the fluctuation analysis, the structures were fitted on the more rigid part of the protein (residues 282–324 and 372–434 of PPARα and 274–316 and 364–426 of RXRα) excluding the residues around the LBP. The fitting and the calculation of RMSFs were done separately for each monomer. The statistical significance of the ligand binding induced difference of average RMSF values of each residue was tested with the classical two-tailed *t*-test. In Figure 4, the areas of the proteins that showed decreased fluctuations in the simulations upon ligand binding are colored blue and the areas, which showed increased fluctuations upon ligand binding are colored red. Residues colored in dark blue and dark red showed averaged fluctuations, which were different in the simulations with and without ligand at 95% confidence level (P-value $<$ 0.05).

The method was validated performing same analysis for the monomer simulations and comparing the result to the NMR[39] and amide HDX[11] measurements of ligand binding to PPARγ. The results indicate that the MD simulations of this study are capable of describing the main features of the ligand-induced stabilization of the PPARα LBD. For details see Supporting Information (Fig. S5).

The RMSF analyses showed that binding of 9cRA to the RXRα LBP stabilizes helices 3 and 10 and the helix 8–9 loop of PPARα [Fig. 4(A,B)]. At the coactivator protein binding site of PPARα, the fluctuations are smaller when both ligands bind to the heterodimer [Fig. 4(E)] compared to GW-bound PPARα [Fig. 4(C)]. When both ligands are bound, large areas in the upper part of the RXRα LBD, namely the helices 5, 7, and 10/11, and the PPARα helix 8–9 loop, helix 10/11 and helices 3 and 4 at the coactivator peptide binding site of PPARα are more stable [Fig. 4(E,F)]. This decrease in fluctuations in the PPARα LBD is a result of conformational and dynamical changes at the dimerization surface caused by ligand binding to the RXRα LBP.

Binding of 9cRA to RXRα decreases fluctuations of RXRα helices 5, 7, 10 and the N-terminal half of helix 11 [Fig. 4(A,B) and Fig. 4(E,F) compared to Fig. (C,D)]. The ligand-induced decrease in fluctuations forms a continuous area of residues extending from RXRα over the heterodimer interface to the helix 10/11 and the helix 8–9 loop, which are located at the heterodimer interface, and further to helix 4/5 and helix 3 of PPARα. When GW is bound to PPARα, similar increase of stability is seen in the N-terminal part of helix 10/11, the helix 8–9 loop and helix 4/5 of RXRα, but in contrast to PPARα, the fluctuations of helix 3 at the coactivator binding site of RXRα were increased. Thus, the MD simulations showed that 9cRA binding to RXRα stabilizes the coactivator binding site of PPARα by a helix 12 independent allosteric mechanism and that this allosteric communication is somewhat asymmetrical as binding of PPARα ligand leads to a weaker and somewhat different effect on RXRα.

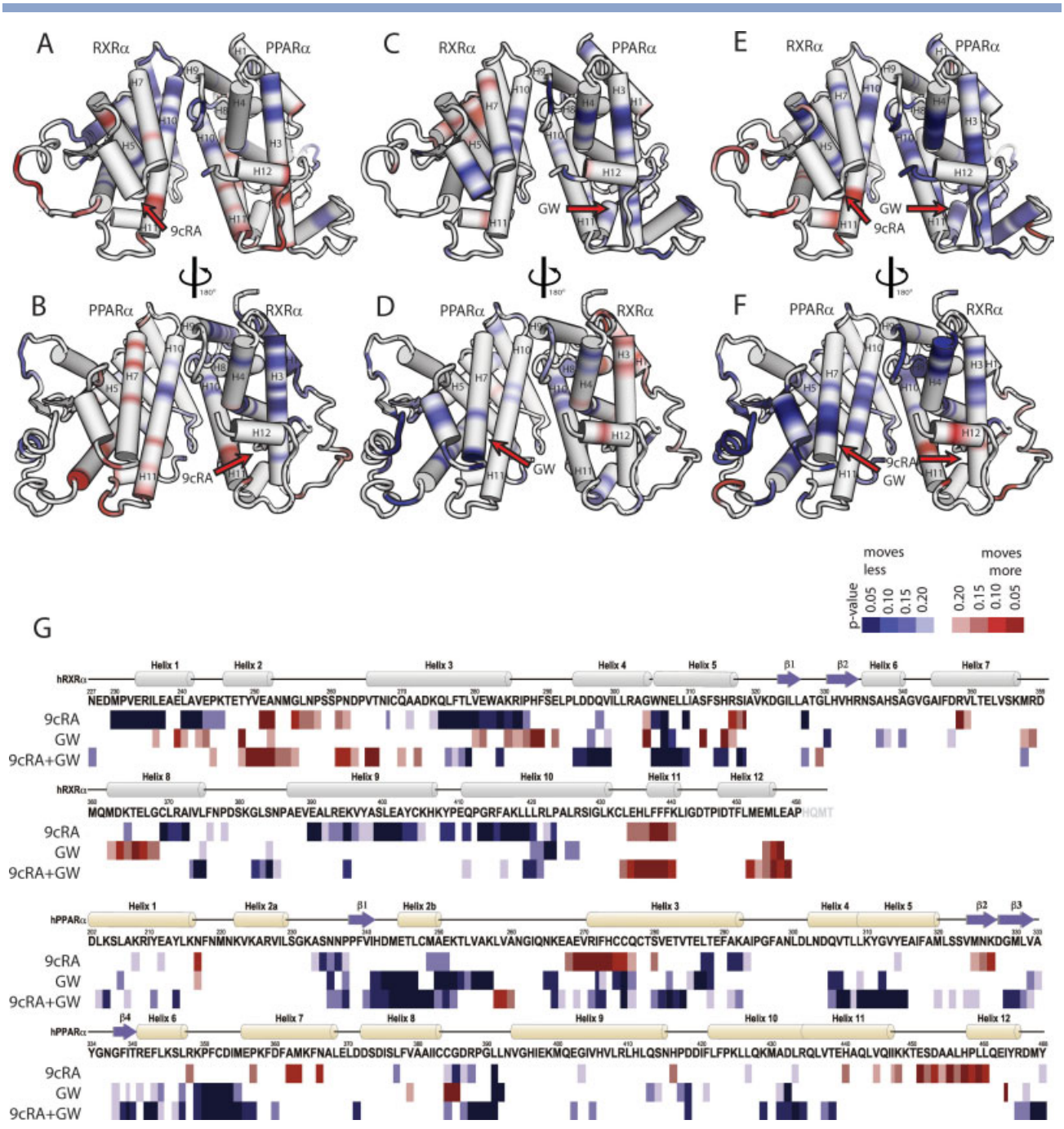

Figure 4

RMSF analyses of the PPARα-RXRα heterodimer MD simulations. Colors: Decrease in the fluctuations upon ligand binding in confidence levels from 80 to 95% (*P*-values 0.20 to 0.05) is indicated with light blue to blue, and similar increase in the fluctuations with orange to red. Areas where the change in the fluctuations was below the confidence level of 80% are colored white. Coactivator binding site is between the helices 3, 4, and 12. The amount of stabilization varies up to 20%, and the highest decreases of fluctuations are located on the dark blue areas with the lowest *P*-values. (**A**,**B**) Effect of 9cRA binding to RXRα compared to apo simulations. (B: rotated view, PPARα on the left.) Ligand binding to RXRα stabilizes RXRα, but also helix 3 at the coactivator binding site of PPARα. (**C**,**D**) Effect of GW binding to PPARα compared to apo simulations. GW stabilizes residues around the LBP and the coactivator binding site. (**E**,**F**) Simulations with two ligands compared to apo simulations. The stabilization at the coactivator binding site (E) is stronger than the stabilization with only PPARα ligand (C). (**G**) The same data shown on the sequence. 9cRA: simulations with 9cRA compared to apo simulations. GW409544: simulations with GW409544 compared to apo simulations. 9cRA + GW409544: Simulations with both ligands compared to apo simulations. The averages of the actual RMSF values are shown in Supporting Information Figure S7 and S8.

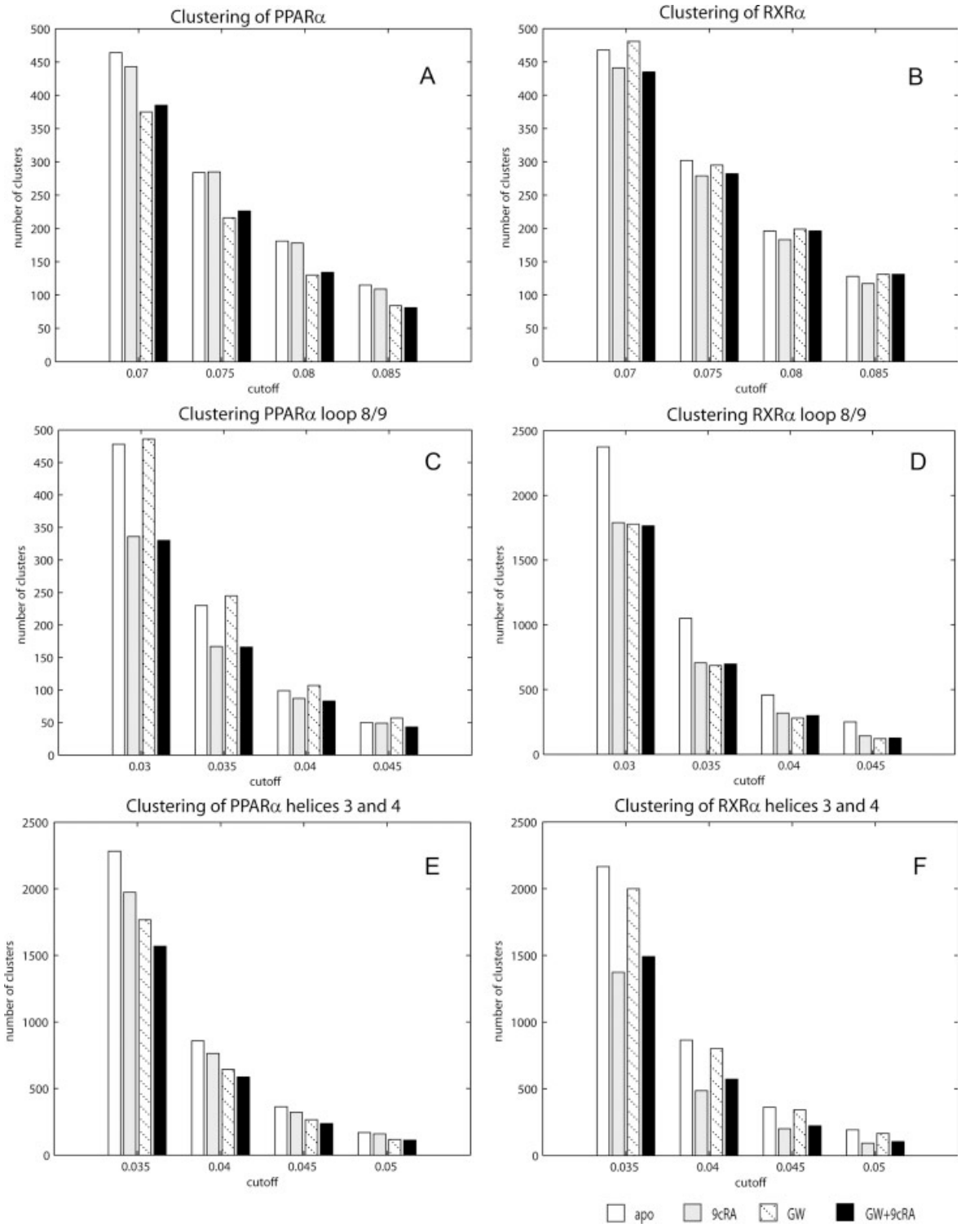

Figure 5

RMSD clustering of LBD, loop 8/9 and helices 3–4 at the coactivator peptide binding site of PPARα and RXRα in the heterodimer MD simulations. Red: no ligands, orange: 9cRA bound to RXRα, blue: GW409544 bound to PPARα, green: both ligands. (**A**) Clustering of the whole PPARα LBD show smallest number of clusters in simulations with PPARα ligand (blue and green). (**B**) Clustering of the whole RXRα LBD show smallest number of clusters in the simulations with RXRα ligand (orange and green). (**C**) Clustering of PPARα loop 8/9 gives similar pattern than B, indicating that the PPARα loop 8/9 is reacting on RXRα ligand, but not on PPARα ligand. (**D**) Clustering of RXRα loop 8/9 shows that it reacts on PPARα ligand if no ligand is bound to RXRα (red compared to blue bar), but also on RXRα ligand (red compared to orange bar). Only weak stabilization with both ligands compared to only RXRα ligand is seen. (**E**) Clustering of helices 3 and 4 at the coactivator binding site of PPARα. Both RXRα and PPARα ligands can stabilize the binding site, and the stabilization is additive: after strong stabilization with PPARα ligand (red and blue bars) the coactivator binding site is still stabilized by RXRα ligand (green bar). (**F**) Clustering of helices 3 and 4 at the coactivator binding site of RXRα. This area is stabilized by PPARα and RXRα ligands, but if RXRα ligand is bound PPARα ligand cannot stabilize the RXRα coactivator binding site any further.

Preorganization of the coactivator binding site of PPARα by RXRα ligand binding

The dynamics of the PPARα-RXRα heterodimer was further analyzed with a cut-off-based RMSD clustering method.[40] In this method, a small number of clusters indicate small mobility or regular motions between a small number of conformations. The composition of the clusters does not necessarily represent any reasonable minimum energy structure, so the contents of the clusters were not further analysed, but the number of clusters was used as a measure of mobility or preorganization.

The clustering was performed for the whole LBD, for the coactivator binding sites and for the helix 8–9 loop located between the coactivator binding site and the heterodimerization interface. For the whole LDBs, larger cut-off values were needed than for clustering of the coactivator binding sites or the helix 8–9 loop, because larger number of atoms and higher flexibility led to larger RMSD values between the structures. All the clusterings were performed with several cut-off values to estimate the sensitivity of the method to the cut-off value. Parallel trajectories, 10 for each system, were pooled to maximize the amount of data in the clustering.

The clustering of the PPARα residues 202–229 and 268–468, excluding the flexible loop area showed a clear difference between systems with and without GW bound to PPARα: in the GW and GW + 9cRA simulations the PPARα had a smaller number of clusters than in the apo or 9cRA simulations with all the tested cut-off values [Fig. 5(A)]. This indicates, in line with the fluctuation analyses, that ligand binding to PPARα clearly restrains the movements of PPARα. Similar results were obtained when RXRα residues 227–241 and 264–458 were clustered: in the 9cRA and GW + 9cRA simulations the RXRα had a smaller number of clusters than in the apo or GW simulations [Fig. 5(B)]. However, 9cRA binding to RXRα had a less pronounced effect on RXRα dynamics than GW binding had on the PPARα LBP. With the two largest cut-off values the difference in the number of clusters in structures from apo- and GW + 9cRA simulations disappeared. In conclusion, the overall movements of the receptor as a whole are controlled by its own ligand, being more notable for PPARα than RXRα.

Next, clustering was performed for the helix 8–9 loop, which is located between the heterodimer interface and helix 3 of the coactivator binding site. The effect of ligand binding on the number of helix 8–9 loop clusters of PPARα (residues 383–394) was, surprisingly, similar to that obtained for the RXRα LBD [Fig. 5(B)]: the number of clusters was smallest in the simulations with 9cRA [Fig. 5(C)], whereas binding of ligand to PPARα LBP did not affect the number of clusters at all. The helix 8–9 loop of RXRα behaves differently: the largest number of clusters was seen in the apo simulations, whereas in all the other simulation systems the number of clusters was similar [Fig. 5(D)]. In addition, there was clearly a smaller number of clusters for the helix 8–9 loop of PPARα than for the same loop in RXRα, indicating higher rigidity for the helix 8–9 loop of PPARα. Thus, this analysis shows that the helix 8–9 loop of PPARα is controlled by RXRα ligand 9cRA and GW has no effect on the loop. The corresponding RXRα loop (residues 376–387) reacts also to 9cRA, presumably making further stabilization with GW difficult when 9cRA is already bound to the RXRα LBP [Fig. 5(D)].

Clustering was also performed for helices 3 and 4 (residues 282–293 and 302–311) of the coactivator binding sites of PPARα, which was found to be stabilized by RXRα ligand binding in the RMSF analyses [Fig. 4(A)]. Clustering of helices 3 and 4 showed that compared to the apo simulations, ligand binding to PPARα LBP decreases the number of clusters notably [Fig. 5(E)]. However, exactly the same is true for the binding of 9cRA to the RXRα LBP and, interestingly, the effects of these two ligands on helix 3 and 4 clusters of PPARα is additive. Corresponding, although clearly smaller, stabilization of RXRα's coactivator binding site (residues 274–285 and 294–303) was seen by PPARα ligand when compared to the apo case, but no decrease was seen when 9cRA was already bound to RXRα [Fig. 5(F)].

The RMSD clustering analysis shows that even though GW controls the structure and motions of PPARα as a whole, 9cRA binding to RXRα has a strong stabilizing effect on the coactivator peptide binding site of PPARα and on the helix 8–9 loop, which is located between the coactivator binding site and RXRα. The corresponding helix 8–9 loop of RXRα is also stabilized by the PPARα ligand, and stabilization by PPARα ligand is also seen at the coactivator binding site of RXRα. However, the helix 8–9 loop of RXRα also reacts to its own ligand, and cannot be further stabilized by PPARα ligand when 9cRA is already bound. This is seen at the coactivator binding site of RXRα as well: the coactivator binding site of RXRα is slightly more stable with PPARα ligand than without, but when 9cRA is bound, no extra stabilization is gained by PPARα ligand binding.

If the ligand binding induced changes seen in the clustering analysis are really connected to the permissive and synergistic activation of PPARα-RXRα system, similar intermonomeric communication should not be seen in the nonpermissive NR heterodimer. To test this, calculations were done for the nonpermissive VDR-RXRα heterodimer with 9cRA as a RXRα ligand and vitamin D3 as a VDR ligand using the same MD simulation and clustering protocols that were used for the PPARα-RXRα heterodimer. It was found that RXRα showed similar behavior in all the ligand conditions in both heterodimer systems, whereas 9cRA binding did not induce notable changes in the behavior of VDR. The difference was especially notable in the helix 8–9 loop, which in the case of

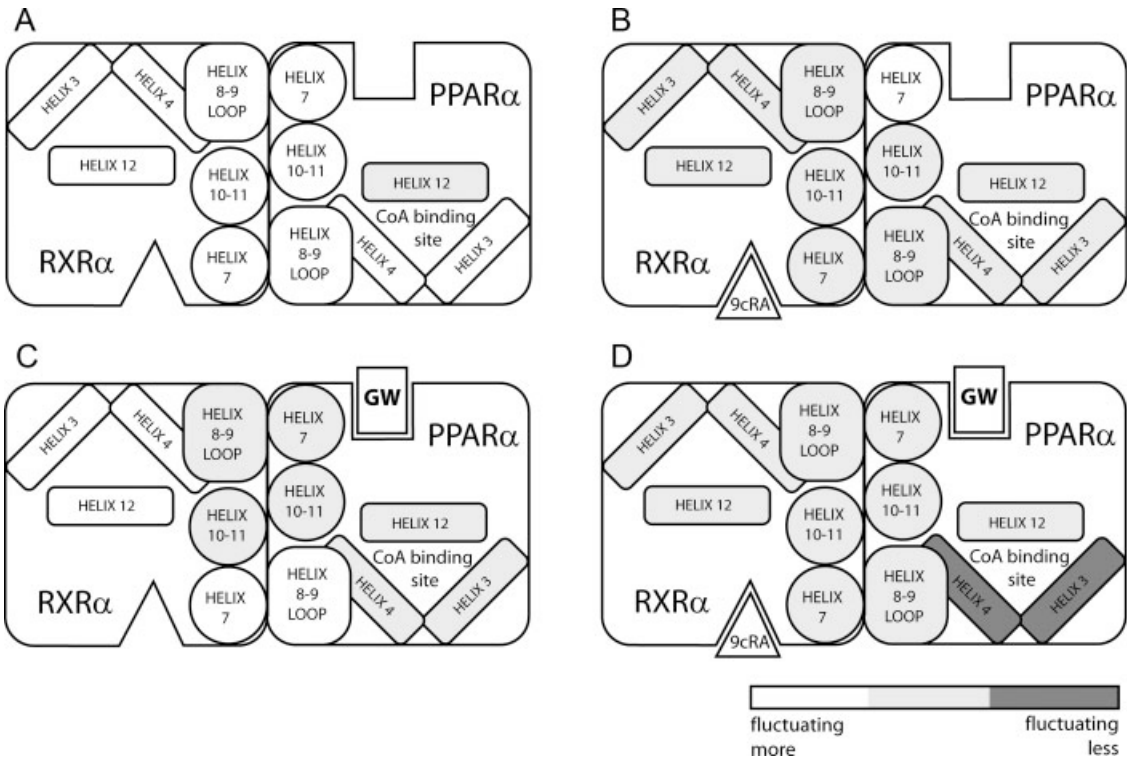

Figure 6

Model of PPARα-RXRα heterodimer activation. (**A**) Stability of PPARα helix 12 makes the system constitutively active. (**B**) 9cRA binding leads to permissive activation by stabilizing the coactivator binding site. (**C**) Binding of GW also stabilizes the coactivator binding site. Even thought not seen in these simulations, stabilization of the helix 12 can play a big role in the activation, depending on the ligand type.[11] (**D**) Combined effects of both ligands lead to the maximum activation.

VDR did not at all respond to 9cRA binding to RXRα (Supporting Information Fig. S6).

DISCUSSION

The activity of permissive NRs can be regulated also by the ligand of the partner receptor, which is often RXRα, and the heterodimeric complex gives full response when both monomers bind their respective ligands. This type of complex functionality requires the presence of long-range allosteric communication between the LBP of one NR and the LBD of the other NR. At the example of the PPARα-RXRα heterodimer the mechanism of allosteric coupling was investigated in this study. We used MD simulations of PPARα and RXRα LBD monomers as well as PPARα-RXRα LBD heterodimers with different combinations of 9cRA (RXRα ligand) and GW (PPARα ligand) occupying the LBPs of the receptor monomers.

The conformation and dynamics of the C-terminal helix 12 is known to be important for the activity of most of the NRs. Stabilization of helix 12 in the agonistic conformation against the main body of the receptor is needed for recruitment of coactivator proteins. However, when helix 12 is stabilized into the correct position by an agonist, or when the agonistic position is stable without an agonist, other parts of the coactivator binding site of NR are important for activation as well. This is shown by computer simulations of a mutated GR,[12] by X-ray structures of PPARα/γ agonists that do not make direct contacts with helix 11 or 12[14,15] and by HDX measurements, which showed that PPARγ activation by partial agonists does not necessarily correlate with helix 12 stabilization.[11] In the latter case, the helix 12 independent activation seems to be related to stabilization of helices 3 and 4, which form the two other sides of the coactivator binding cleft, and the β-sheet region. In addition, the distinct functional properties of selective PPARγ modulators have been linked to a helix 12 independent mechanism and subtle changes influencing the dynamics of the LBD.[41]

In our computer simulations of the PPARα-RXRα heterodimer an allosteric signal transmission was seen between the LBP of RXRα and the coactivator binding site of PPARα. Namely, when 9cRA was bound to the RXRα LBP, notable stabilization of helices 3 and 4 at the coactivator binding site of PPARα was observed [Figs. 5(A) and 6(E)]. It was also seen that even though bind-

ing of GW stabilizes the coactivator site of PPARα, binding of 9cRA to RXRα can stabilize it further. The stabilization was seen in the reduced RMSF values and smaller number of clusters in the structural clustering analysis. The binding of RXRα ligand led to small changes in the average positions of helix 7 and helix 11, seen in decreased helix 11 - helix 11 and helix 7–C-terminus distances over the heterodimer interface. Thus, these structural changes increased packing of the heterodimerization interface and enhanced propagation of the ligand-induced structural/dynamical changes from RXRα LBD over the interface to PPARα.

The effect of RXRα ligand binding on PPARα is clearly seen in the behavior of the PPARα's helix 8–9 loop, which is located at the heterodimer interface between RXRα and the coactivator binding site of PPARα. Although the PPARα LBD as a whole is stabilized by its own ligand [Fig. 5(A)], the clustering analysis showed that the movements of the PPARα helix 8–9 loop is controlled by RXRα ligand binding [Fig. 5(C)].

Similarly to PPARα, the helix 8–9 loop and the coactivator binding site of RXRα reacts to ligand binding to PPARα LBP [Fig. 5(D,F)]. However, the helix 8–9 loop of RXRα reacts also to RXRα ligand binding [Fig. 5(D)]. In addition, it is also visible that ligand binding to the PPARα LBP, if 9cRA already occupies RXRα LBP, does not further stabilize the helix 8–9 loop [Fig. 5(D)]. The stabilization of RXRα coactivator binding site is markedly different from that observed for PPARα: a notable decrease in the number of clusters is seen only when RXRα's own ligand is bound, and no further decrease is caused by PPARα ligand binding [Fig. 5(F)]. The functional model from this comparison shows that although there are some similarities between RXRα and PPARα with respect to ligand binding to partner protein, a synergistic effect is seen only in the case of PPARα. In addition, the absence of RXRα ligand binding-induced changes in the simulations of the nonpermissive RXRα-VDR system supports the conclusion that a helix 12 independent mechanism seen in the PPARα-RXRα simulations has a role in allosteric activation of NRs.

On the basisi of the results of this work, we created a simplified model of PPARα-RXRα heterodimer activation (Fig. 6). If LBPs of both PPARα and RXRα are unoccupied, stability of PPARα helix 12 makes the system constitutively active [Fig. 6(A)]. Binding of 9cRA decreases fluctuations of large parts of RXRα [Fig. 6(B)]. Increased packing at the heterodimer interface and decreased fluctuations of RXRα helices 10–11 and 7 stabilize those areas of PPARα, which they are in contact with: helix 10/11 and the helix 8–9 loop. The helix 8–9 loop is in contact with the helix 4 of the coactivator binding site. The fluctuations at the coactivator binding site are decreased, which preorganizes the system for coactivator binding and the system displays permissive activation. Binding of GW also stabilizes the coactivator binding site [Fig. 6(C)]. Helix 12 stabilization upon GW binding was not seen in these simulations, but depending on the type of ligand, helix 12 is expected to be more stable as well (not shown in the model).[11] Helices 3 and 4 of RXRα are not stabilized. Combined effect of GW and 9cRA lead to strong stabilization of the coactivator binding site and the system displays synergistic effect [Fig. 6(D)].

The recent long-awaited crystal structure of the full-length PPARγ-RXRα complex on DNA provided important data on the domain organization of the heterodimer in 3D space leading to functional implications, but it was unable to provide a direct explanation for the phantom ligand effect or for receptor permissivity.[38] The MD simulations suggested that the allosteric signaling between the monomers results from subtle structural and dynamical changes of the whole heterodimerization surface rather than on individual residues. This observation was supported by mutation data presented here: large set of mutations on the heterodimerization interface affect signal transmission.

The data in this study suggests that allosteric activation of the PPARα-RXRα heterodimer is due to relatively small structural and dynamical ligand binding-induced changes rather than large conformational changes in the heterodimer structure. This mechanism is reminiscent of the dynamic allostery model of the cooperative oxygen binding to hemoglobin proposed by Yonetani and Laberge.[2] According to this model, the dynamics of hemoglobin rather than quaternary structural changes play the central role in regulation of oxygen affinity. The cooperativity is due to a decrease in hemoglobin backbone flexibility caused by hydrogen bonding or steric hindrance by the ligand, which leads to increased reactivity of the heme. Analysis of long MD trajectories by methods based on cross-correlation and various amino acid network analyses have been used to obtain detailed knowledge about allosteric mechanism and communication pathways in protein systems.[42–46] Such analysis methods could also be applied to obtain more detailed picture on the allosteric mechanism and identify possible residue level communication pathways in NR systems. It is likely that increased possibilities to use MD simulations for large proteins will reveal that protein motions have a more widespread role in the mechanisms of allosteric systems. The understanding of allosteric mechanisms may in fact, as suggested in the recent paper from Lee *et al.*, lead to creation of regulatory activities into engineered multidomain protein systems.[47]

The statistical coupling analysis (SCA) is a sequence analysis method designed to detect coevolution of position pairs in protein sequences.[48] Because coevolution of two positions is likely to be driven by functional interaction of the residues, it is likely that such residue pairs are involved in allosteric networks. It has been shown that results of SCA are consistent with the known allosteric mechanisms in several protein families.[48,49] SCA has been applied to

study the allosteric ligand activation (i.e., permissivity) in RXRα heterodimers of several NRs and predicted a group of amino acid residues outside the helix 12 that are important for allosteric signaling in NR heterodimers.[3] Functional analysis of these residues demonstrated that they belonged to an allosteric network as their mutation weakened or destroyed RXRα agonist induced allosteric activation of several permissive NRs.[3] These amino acid residues are located mainly in helices 3 and 4 and the helix 8–9 loop. The same region, the upper half of PPARα, was seen to be stabilized by 9cRA binding to RXRα LBP. Also, the number of clusters of helix 8–9 loop and the helices 3 and 4 were observed to decrease in response to ligand binding to RXRα LBP in this study.

The results of this study suggest that permissive and synergistic activation of the PPARα-RXRα heterodimer is mediated by the same mechanism: stabilization of the PPARα coactivator peptide binding site, which is a result of conformational changes in both LBDs caused by ligand binding. The overall ability of a NR heterodimer to respond to RXRα ligand can be dependent on the stability or rigidity of its coactivator binding site. HDX measurements show that this stability can be modulated by ligands.[11] It would be interesting to see, whether PPARγ shows reduced synergistic activation with the helix 3 stabilizing partial agonists, such as BVT.13, when compared to ligands that do not stabilize helix 3.

CONCLUSIONS

The allosteric activation of the PPARα-RXRα heterodimer LBDs was studied with MD simulations in the apo form, and in complex with 9cRA, GW and with both 9cRA and GW. Ligand binding to RXRα was seen to decrease fluctuations on a continuous area of residues extending from the ligand binding pocket of RXRα through the helix 8–9 loop of PPARα, which is located at the heterodimerization interface, to the helices 3 and 4 at the coactivator binding site of PPARα. The function of the residues identified from MD simulation was tested experimentally, providing evidence that the exchange of information within the heterodimer involves a complex network with alternative, substitutable interactions. These results suggest a helix 12 independent mechanism for permissive and synergistic activation of NR heterodimers by coactivator binding site stabilization.

REFERENCES

1. Jensen AA, Spalding TA. Allosteric modulation of G-protein coupled receptors. Eur J Pharm Sci 2004;21:407–420.
2. Yonetani T, Laberge M. Protein dynamics explain the allosteric behaviors of hemoglobin. Biochim Biophys Acta Proteins Proteomics 2008;1784:1146–1158.
3. Shulman AI, Larson C, Mangelsdorf DJ, Ranganathan R. Structural determinants of allosteric ligand activation in RXR heterodimers. Cell 2004;116:417–429.
4. Aranda A, Pascual A. Nuclear hormone receptors and gene expression. Physiol Rev 2001;81:1269–1304.
5. Bain DL, Heneghan AF, Connaghan-Jones KD, Miura MT. Nuclear receptor structure: implications for function. Annu Rev Physiol 2007;69:201–220.
6. Xie W, Evans RM. Orphan nuclear receptors: the exotics of xenobiotics. J Biol Chem 2001;276:37739–37742.
7. Nettles KW, Greene GL. Ligand control of coregulator recruitment to nuclear receptors. Annu Rev Physiol 2005;67:309–333.
8. Kallenberger BC, Love JD, Chatterjee VK, Schwabe JW. A dynamic mechanism of nuclear receptor activation and its perturbation in a human disease. Nat Struct Biol 2003;10:136–140.
9. Frank C, Gonzalez MM, Oinonen C, Dunlop TW, Carlberg C. Characterization of DNA complexes formed by the nuclear receptor constitutive androstane receptor. J Biol Chem 2003;278:43299–43310.
10. Molnar F, Matilainen M, Carlberg C. Structural determinants of the agonist-independent association of human peroxisome proliferator-activated receptors with coactivators. J Biol Chem 2005;280:26543–26556.
11. Bruning JB, Chalmers MJ, Prasad S, Busby SA, Kamenecka TM, He Y, Nettles KW, Griffin PR. Partial agonists activate PPARγ using a helix 12 independent mechanism. Structure 2007;15:1258–1271.
12. Carlsson P, Koehler KF, Nilsson L. Glucocorticoid receptor point mutation V571M facilitates coactivator and ligand binding by structural rearrangement and stabilization. Mol Endocrinol 2005;19:1960–1977.
13. Burendahl S, Treuter E, Nilsson L. Molecular dynamics simulations of human LRH-1: the impact of ligand binding in a constitutively active nuclear receptor. Biochemistry (Mosc) 2008;47:5205–5215.
14. Östberg T, Svensson S, Selen G, Uppenberg J, Thor M, Sundbom M, Sydow-Backman M, Gustavsson AL, Jendeberg L. A new class of peroxisome proliferator-activated receptor agonists with a novel binding epitope shows antidiabetic effects. J Biol Chem 2004;279:41124–41130.
15. Oberfield JL, Collins JL, Holmes CP, Goreham DM, Cooper JP, Cobb JE, Lenhard JM, Hull-Ryde EA, Mohr CP, Blanchard SG, Parks DJ, Moore LB, Lehmann JM, Plunket K, Miller AB, Milburn MV, Kliewer SA, Willson TM. A peroxisome proliferator-activated receptor gamma ligand inhibits adipocyte differentiation. Proc Natl Acad Sci USA 1999;96:6102–6106.
16. Schräder M, Nayeri S, Kahlen JP, Müller KM, Carlberg C. Natural vitamin-D-3 response elements formed by inverted palindromes - polarity-directed ligand sensitivity of vitamin-D-3 receptor retinoid-X receptor heterodimer-mediated transactivation. Mol Cell Biol 1995;15:1154–1161.
17. Willson TM, Brown PJ, Sternbach DD, Henke BR. The PPARs: from orphan receptors to drug discovery. J Med Chem 2000;43:527–550.
18. Xu HE, Lambert MH, Montana VG, Plunket KD, Moore LB, Collins JB, Oplinger JA, Kliewer SA, Gampe RT, Mckee DD, Moore JT, Willson TM. Structural determinants of ligand binding selectivity between the peroxisome proliferator-activated receptors. Proc Natl Acad Sci USA 2001;98:13919–13924.
19. Lindahl E, Hess B, Van Der Spoel D. GROMACS 3.0: a package for molecular simulation and trajectory analysis. J Mol Model 2001;7:306–317.
20. Schuler LD, Daura X, Van Gunsteren WF. An improved GROMOS96 force field for aliphatic hydrocarbons in the condensed phase. J Comput Chem 2001;22:1205–1218.
21. Hess B, Bekker H, Berendsen HJC, Fraaije JGEM. LINCS: a linear constraint solver for molecular simulations. J Comput Chem 1997;18:1463–1472.
22. Miyamoto S, Kollman PA. Settle—an analytical version of the shake and rattle algorithm for rigid water models. J Comput Chem 1992;13:952–962.

23. Tironi IG, Sperb R, Smith PE, Vangunsteren WF. A generalized reaction field method for molecular-dynamics simulations. J Chem Phys 1995;102:5451–5459.
24. Heinz TN, Van Gunsteren WF, Hunenberger PH. Comparison of four methods to compute the dielectric permittivity of liquids from molecular dynamics simulations. J Chem Phys 2001;115: 1125–1136.
25. Berendsen HJC, Postma JPM, Van Gunsteren WF, Dinola A, Haak JR. Molecular-dynamics with coupling to an external bath. J Chem Phys 1984;81:3684–3690.
26. Sher T, Yi HF, Mcbride OW, Gonzalez FJ. Cdna cloning, chromosomal mapping, and functional-characterization of the human peroxisome proliferator activated receptor. Biochemistry (Mosc) 1993; 32:5598–5604.
27. Mangelsdorf DJ, Ong ES, Dyck JA, Evans RM. Nuclear receptor that identifies a novel retinoic acid response pathway. Nature 1990; 345:224–229.
28. Carlberg C, Bendik I, Wyss A, Meier E, Sturzenbecker LJ, Grippo JF, Hunziker W. 2 nuclear signaling pathways for vitamin-D. Nature 1993;361:657–660.
29. Teboul M, Enmark E, Li Q, Wikstrom AC, Peltohuikko M, Gustafsson JA. Or-1, a member of the nuclear receptor superfamily that interacts with the 9-*cis*-retinoic acid receptor. Proc Natl Acad Sci USA 1995;92:2096–2100.
30. Petkovich M, Brand NJ, Krust A, Chambon P. A human retinoic acid receptor which belongs to the family of nuclear receptors. Nature 1987;330:444–450.
31. Choi HS, Chung MR, Tzameli I, Simha D, Lee YK, Seol W, Moore DD. Differential transactivation by two isoforms of the orphan nuclear hormone receptor CAR. J Biol Chem 1997;272:23565–23571.
32. Schmidt A, Endo N, Rutledge SJ, Vogel R, Shinar D, Rodan GA. Identification of a new member of the steroid-hormone receptor superfamily that is activated by a peroxisome proliferator and fatty-acids. Mol Endocrinol 1992;6:1634–1641.
33. Mascaro C, Acosta E, Ortiz JA, Marrero PF, Hegardt FG, Haro D. Control of human muscle-type carnitine palmitoyltransferase I gene transcription by peroxisome proliferator-activated receptor. J Biol Chem 1998;273:8560–8563.
34. Kahlen JP, Carlberg C. Functional characterization of a 1,25-dihydroxyvitamin D-3 receptor binding site found in the rat atrial natriuretic factor promoter. Biochem Biophys Res Commun 1996;218: 882–886.
35. Honkakoski P, Zelko I, Sueyoshi T, Negishi M. The nuclear orphan receptor CAR-retinoid X receptor heterodimer activates the phenobarbital-responsive enhancer module of the CYP2B gene. Mol Cell Biol 1998;18:5652–5658.
36. Toell A, Kroncke KD, Kleinert H, Carlberg C. Orphan nuclear receptor binding site in the human inducible nitric oxide synthase promoter mediates responsiveness to steroid and xenobiotic ligands. J Cell Biochem 2002;85:72–82.
37. Gampe RT, Montana VG, Lambert MH, Miller AB, Bledsoe RK, Milburn MV, Kliewer SA, Willson TM, Xu HE. Asymmetry in the PPARγ/ RXRα crystal structure reveals the molecular basis of heterodimerization among nuclear receptors. Mol Cell 2000;5:545–555.
38. Chandra V, Huang PX, Hamuro Y, Raghuram S, Wang YJ, Burris TP, Rastinejad F. Structure of the intact PPARγ-RXRα nuclear receptor complex on DNA. Nature 2008;456:350–356.
39. Johnson BA, Wilson EM, Li Y, Moller DE, Smith RG, Zhou G. Ligand-induced stabilization of PPARγ monitored by NMR spectroscopy: implications for nuclear receptor activation. J Mol Biol 2000;298:187–194.
40. Daura X, Van Gunsteren WF, Mark AE. Folding-unfolding thermodynamics of a beta-heptapeptide from equilibrium simulations. Proteins Struct Funct Genet 1999;34:269–280.
41. Einstein M, Akiyama TE, Castriota GA, Wang CF, Mckeever B, Mosley RT, Becker JW, Moller DE, Meinke PT, Wood HB, Berger JP. The differential interactions of peroxisome proliferator-activated receptor gamma ligands with tyr473 is a physical basis for their unique biological activities. Mol Pharmacol 2008;73:62–74.
42. Bradley MJ, Chivers PT, Baker NA. Molecular dynamics simulation of the Escherichia coli NikR protein: equilibrium conformational fluctuations reveal interdomain allosteric communication pathways. J Mol Biol 2008;378:1155–1173.
43. Ghosh A, Vishveshwara S. A study of communication pathways in methionyl-tRNA synthetase by molecular dynamics simulations and structure network analysis. Proc Natl Acad Sci USA 2007;104: 15711–15716.
44. Kormos BL, Baranger AM, Beveridge DL. Do collective atomic fluctuations account for cooperative effects? Molecular dynamics studies of the U1A-RNA complex. J Am Chem Soc 2006;128:8992–8993.
45. Morra G, Verkhivker G, Colombo G. Modeling signal propagation mechanisms and ligand-based conformational dynamics of the Hsp90 molecular chaperone full-length dimer. PLoS Comput Biol 2009;5:e1000323.
46. Sethi A, Eargle J, Black AA, Luthey-Schulten Z. Dynamical networks in tRNA: protein complexes. Proc Natl Acad Sci USA 2009;106: 6620–6625.
47. Lee J, Natarajan M, Nashine VC, Socolich M, Vo T, Russ WP, Benkovic SJ, Ranganathan R. Surface sites for engineering allosteric control in proteins. Science 2008;322:438–442.
48. Suel GM, Lockless SW, Wall MA, Ranganathan R. Evolutionarily conserved networks of residues mediate allosteric communication in proteins. Nat Struct Biol 2003;10:59–69.
49. Hatley ME, Lockless SW, Gibson SK, Gilman AG, Ranganathan R. Allosteric determinants in guanine nucleotide-binding proteins. Proc Natl Acad Sci USA 2003;100:14445–14450.

SUPPLEMENTARY MATERIAL

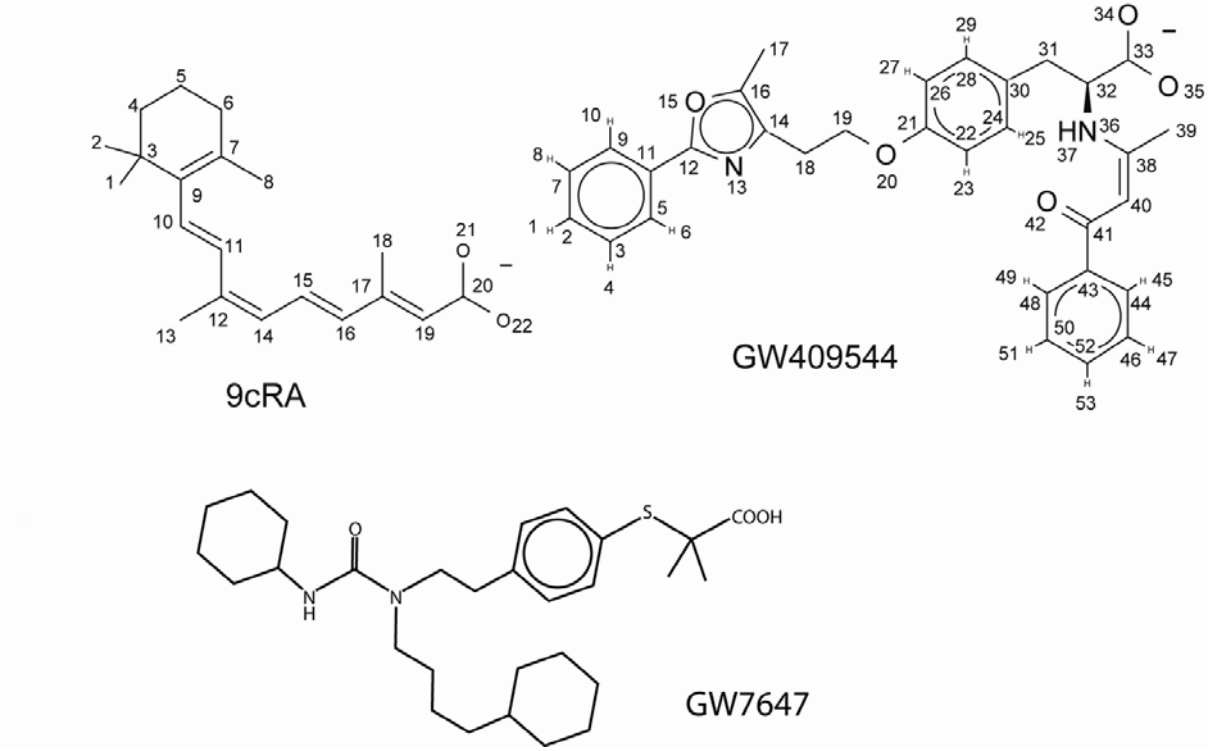

Fig. S1: Structures of 9cRA and the PPARα ligands used in this work. 9cRA is a natural agonist of RXRα. GW409544 and GW7646 are synthetic agonists of PPARα. 9cRA and GW409544 were present in the crystal structures used for the starting coordinates for the simulations.

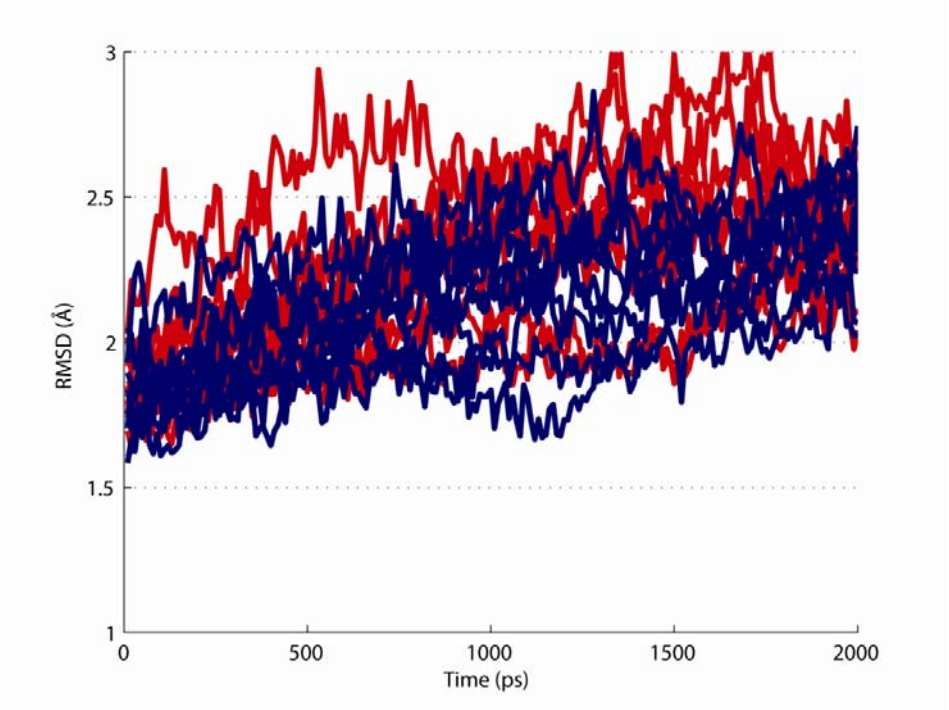

Fig. S2: RMSDs of Cα atoms in PPARα monomer simulations with (blue) and without (red) a ligand. All ten parallel runs of both systems were stable. No differences are observed in simulations with and without a ligand.

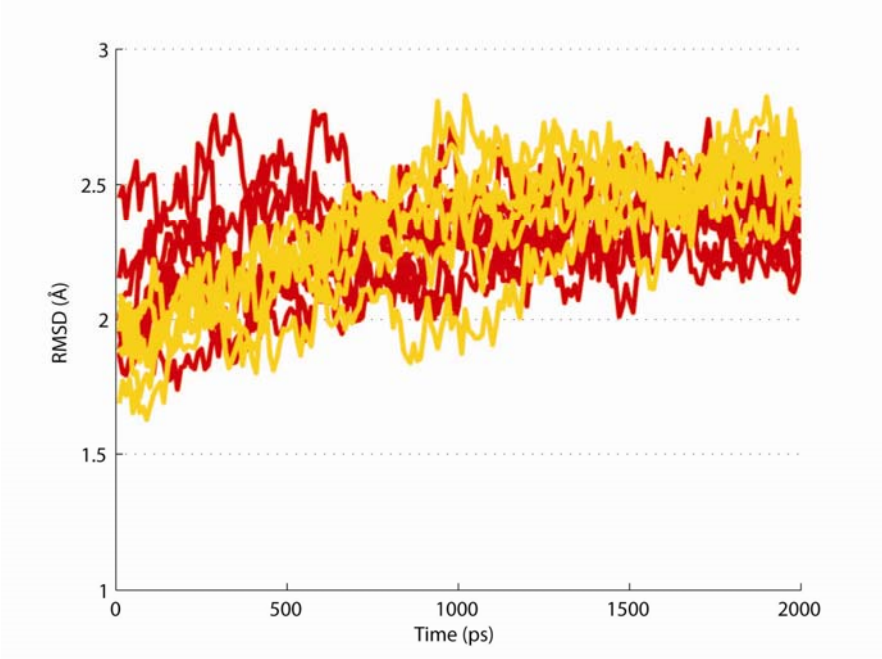

Fig. S3: RMSDs of Cα atoms in RXRα monomer simulations with (orange) and without (red) a ligand. All ten parallel runs of both systems were stable. No differences are observed in simulations with and without a ligand.

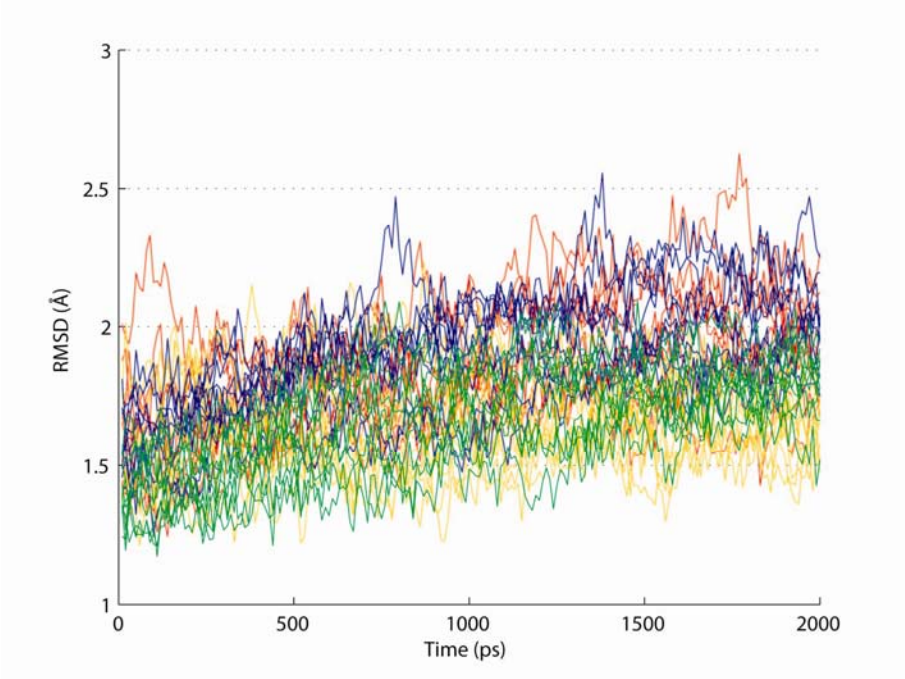

Fig. S4: The Cα RMSDs in the PPARα-RXRα heterodimer simulations. Red: no ligand. Orange: 9cRA bound to RXRα. Blue: GW409544 bound to PPARα. Green: both ligands bound.

Atom numbers in tables S1 to S10 refer to the atoms indicated in Fig. S1. Parameters are given for the GROMOS force-field, in analogy to the 45A3 parameter set.

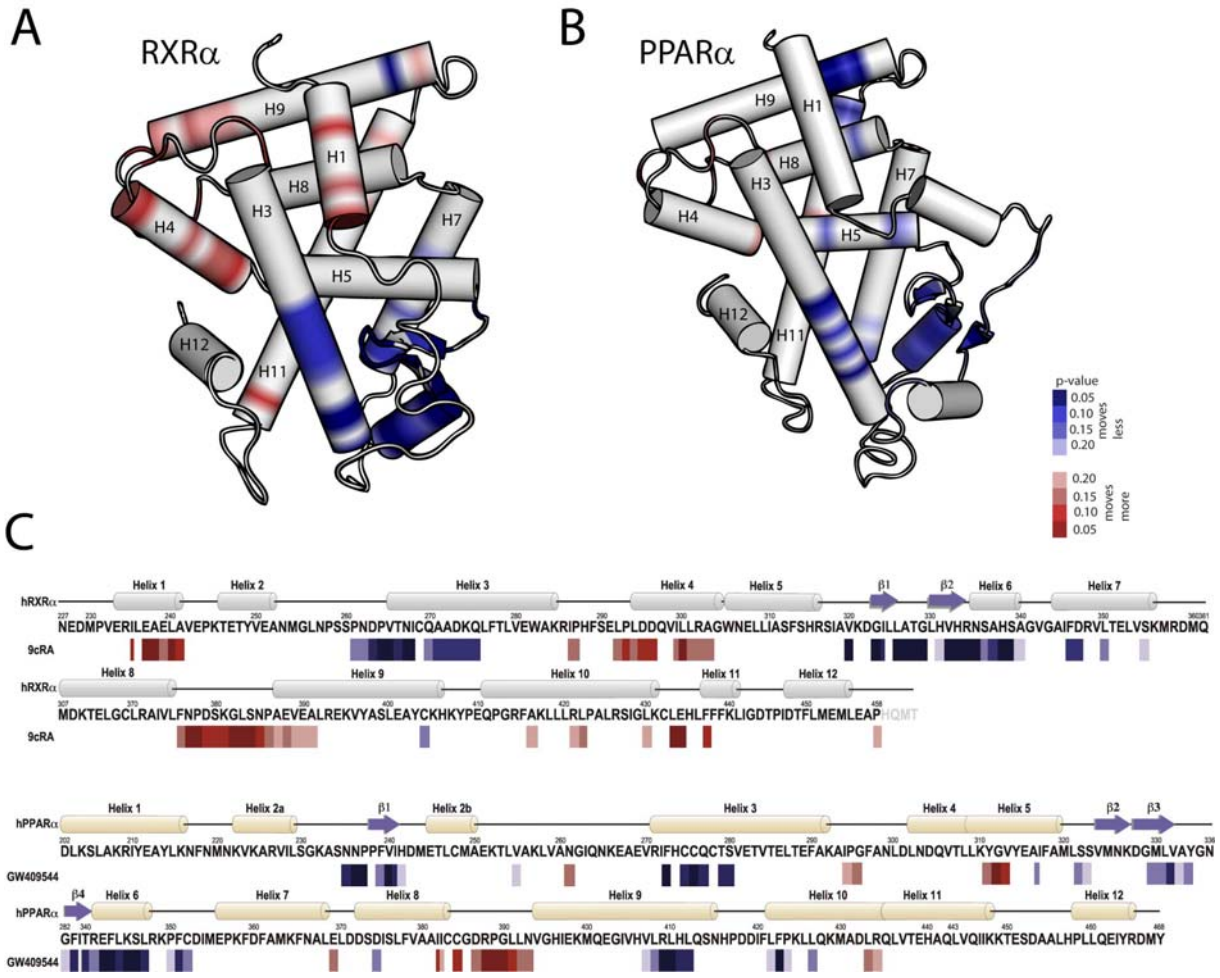

Fig. S5. Ligand-induced changes in atomic fluctuations of PPARα and RXRα monomers in MD simulations. Averages over parallel simulations with and without ligand are compared. Colors: 5-20 % decrease in the fluctuations upon ligand binding is indicated with light blue to blue and similar increase in the fluctuations with orange to red. Areas where the change in the fluctuations was less than 5 % are colored white. 9cRA binding to RXRα decreases fluctuations around the LBP (A). GW409544 binding to PPARα leads to overall stabilization of the LBD. The stabilization of helices 3 and 4 is particularly notable (B).

As expected, the 9cRA binding to RXRα led to stabilization at 95 % confidence level of residues in helices 3, 6, 7 and the β-sheet area, all located around the LBP (Fig. 2A). Surprisingly, helices 1, 4 and the N-terminal half of helix 9 were fluctuating more after 9cRA binding. In PPARα, increased and decreased fluctuations are located mostly at the same parts of the protein as in RXRα. However, in PPARα higher stability is seen on larger areas and increase of fluctuations on smaller areas than in RXRα. In addition to the amino acids around the LBP, a cluster of stabilized amino acid residues is located at the C-terminal part of helix 9 and N-terminal parts of helices 8 and 10 of PPARα. This stabilization is mediated by helix 5, which is located between helix 8 and the LBP. In RXRα, only the C-terminal part of helix 9 from this cluster shows stabilization, but helix 7 in RXRα is more stabilized than helix 7 in PPARα. Thus, ligand binding to PPARα

and RXRα monomers led to similar stabilization of residues close to LBP in both receptors, but in the case of PPARα the stabilization of other parts of the LBD was more pronounced.

Johnson *et al.* studied ligand-induced stabilization of PPARγ with NMR spectroscopy.[39] Their results indicate that apo PPARγ is in a conformationally mobile state and that agonist binding is associated with a marked stabilization of the conformation. The ligand-stabilized areas of the LBD of PPARγ include helices 3 and 4 in the co-activator peptide binding site. These ligand-induced changes in the PPAR structure are in good agreement with our MD simulation results. Also helix 12 of PPARγ was stabilized upon ligand binding in the NMR measurements, but this was not seen in the MD simulations. A likely reason for this is the difference in the time scales of the studies: the motions observed in the NMR experiment were in micro- to milliseconds, whereas the length of the MD simulations was only 2 ns. The MD simulations of this length are not long enough to sample slowly moving areas of the receptor, such as helix 12. Amide HDX showed that agonists stabilized in addition to helix 12 also other parts of the receptor, such as the β-sheet area and helix 3 of the PPARγ LBD.[11] This stabilization, which was also seen in the MD simulations, may explain activity of partial agonists. Taken together, comparison with the NMR and amide HDX results indicate that the MD simulations of this study are capable of describing the main features of the ligand-induced stabilization of the PPARα LBD.

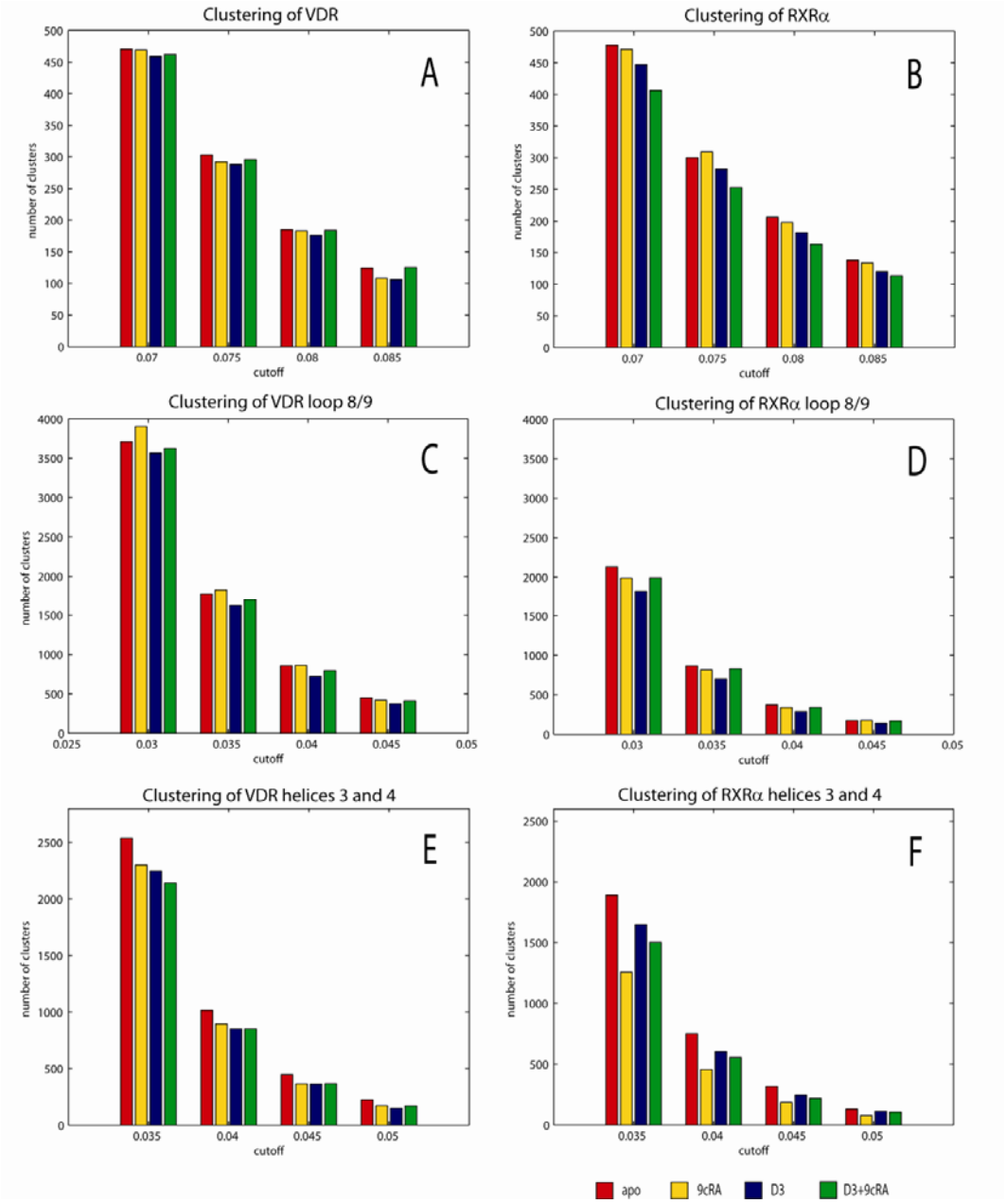

Figure S6. RMSD clustering of LBD, helix 8-9 loop and helices 3-4 at the co-activator peptide binding site of VDR and RXRα in the VDR-RXRα heterodimer MD simulations. Red: no ligands, orange: 9cRA bound to RXRα, blue: D3 bound to VDR, green: both ligands. A: Clustering of the whole VDR LBD shows no decrease in the number of clusters when D3 is bound. B: Clustering of the whole RXRα LBD shows that both ligands decrease fluctuations. C: Clustering of helix 8-9 loop of VDR resemble the clustering of the whole VDR LBD. D: Clustering of the helix 8-9 loop of RXRα gives similar pattern than A and C. E: Clustering of helices 3 and 4 at the co-activator binding site of VDR. Both RXRα and VDR ligands can weakly stabilize the co-activator binding site of VDR. F: Clustering of helices 3 and 4 at the co-activator binding site of RXRα. This area is stabilized mostly by 9cRA. RXRα dynamics in the VDR-RXRα heterodimer (figs S6 B, D, F) in all ligand conditions is similar to that in the PPARα-RXRα heterodimer (Fig 5. B, D, F). The most notable difference is the stronger impact of the VDR ligand on the fluctuations of the whole RXRα LBD. The effect of RXRα ligand binding on VDR is much weaker than on PPARα. For example, at the co-activator binding site of VDR (E), the difference in the number of clusters between the D3 and the D3+9cRA simulations is 4.8 % with cutoff value 0.035 and disappears with smaller cutoff values indicating no synergistic activation with two ligands. The same difference in PPARα simulations is 11.2 % and it is seen with all the cutoff values. The VDR helix 8-9 loop dynamics is not affected by 9cRA.

Table S1. Atom types and atomic charges for 9cRA. Atom types refer to Van der Waals interaction types in the GROMOS 45A3 force field.

Atom	Type	charge
		e
1	14	0
2	14	0
3	45	0
4	44	0
5	44	0
6	44	0
7	11	0
8	14	0
9	11	0
10	16	0
11	16	0
12	11	0
13	14	0
14	16	0
15	16	0
16	16	0
17	11	0
18	14	0
19	16	0
20	13	0.27
21	2	-0.635
22	2	-0.635

Table S2. Bond length parameters for 9cRA.

Bond	Force constant	Bond length
	10^6kJmol^{-1}nm^{-4}	nm
1 - 3	7.15	0.153
2 - 3	7.15	0.153
3 - 4	7.15	0.153
3 - 9	7.15	0.153
4 - 5	7.15	0.153
5 - 6	7.15	0.153
6 - 7	7.15	0.153
7 - 8	7.15	0.153
7 - 9	11.8	0.133
9 - 10	7.64	0.148
10 - 11	10.2	0.136
11 - 12	7.64	0.148
12 - 13	7.15	0.153
12 - 14	10.2	0.136
14 - 15	7.64	0.148
15 - 16	10.2	0.136
16 - 17	7.64	0.148

17 - 18	7.15	0.153
17 - 19	10.2	0.136
19 - 20	7.64	0.148
20 - 21	13.4	0.125
20 - 22	13.4	0.125

Table S3. Bond angle parameters for 9cRA.

Angle	Force constant	Bond Angle
	$kJmol^{-1}$	degree
1 - 3 - 2	520	109.5
1 - 3 - 4	520	109.5
1 - 3 - 9	520	109.5
2 - 3 - 4	520	109.5
2 - 3 - 9	520	109.5
4 - 3 - 9	520	109.5
3 - 4 - 5	520	109.5
4 - 5 - 6	520	109.5
5 - 6 - 7	520	109.5
6 - 7 - 8	560	120
6 - 7 - 9	560	120
8 - 7 - 9	560	120
3 - 9 - 7	560	120
3 - 9 - 10	560	120
7 - 9 - 10	560	120
9 - 10 - 1	560	120
10 - 11 - 12	560	120
11 - 12 - 13	560	120
11 - 12 - 14	560	120
13 - 12 - 14	560	120
12 - 14 - 15	560	120
14 - 15 - 16	560	120
15 - 16 - 17	560	120
16 - 17 - 18	560	120
16 - 17 - 19	560	120
18 - 17 - 19	560	120
17 - 19 - 20	560	120
19 - 20 - 21	635	117
19 - 20 - 22	635	117
21 - 20 - 22	770	126

Table S4. Dihedral angle parameters for 9cRA.

dihedral	Force constant	Phase shift	Multiplicity
	$kJmol^{-1}$		
9 - 3 - 4 - 5	5.92	1	3
4 - 3 - 9 - 7	5.92	1	3
3 - 4 - 5 - 6	5.92	1	3
4 - 5 - 6 - 7	5.92	1	3
5 - 6 - 7 - 9	5.92	1	3
6 - 7 - 9 - 3	33.5	-1	2
7 - 9 - 10 - 11	33.5	-1	2
9 - 10 - 11 - 12	33.5	-1	2
10 - 11 - 12 - 14	16.7	-1	2
11 - 12 - 14 - 15	33.5	-1	2
12 - 14 - 15 - 16	16.7	-1	2
14 - 15 - 16 - 17	33.5	-1	2
15 - 16 - 17 - 19	16.7	-1	2
16 - 17 - 19 - 20	33.5	-1	2
17 - 19 - 20 - 21	1.0	1	6

Table S5. Improper dihedral angle parameters for the 9cRA.

Improper	Force constant	angle
	$kJmol^{-1}degree^{-2}$	degree
7 - 6 - 9 - 8	0.051	0
9 - 3 - 10 - 7	0.051	0
12 - 11 - 14 - 13	0.051	0
17 - 16 - 19 - 18	0.051	0
20 - 19 - 21 - 22	0.051	0

Table S6. Atom types and atomic charges for GW409544. Atom types refer to the Van der Waals types in the GROMOS 45A3 force field.

Atom	Type	Charge
		e
1	17	0.1
2	11	-0.1
3	11	-0.1
4	17	0.1
5	11	-0.1
6	17	0.1
7	11	-0.1
8	17	0.1
9	11	-0.1
10	17	0.1
11	11	0
12	11	0.22
13	8	-0.22
14	11	0.06
15	3	-0.14
16	11	0.08

17	14	0
18	13	0
19	13	0.18
20	3	-0.36
21	11	0.18
22	11	-0.1
23	17	0.1
24	11	-0.1
25	17	0.1
26	11	-0.1
27	17	0.1
28	11	-0.1
29	17	0.1
30	11	0
31	13	0
32	12	0
33	11	0.27
34	2	-0.635
35	2	-0.635
36	10	-0.28
37	18	0.28
38	11	0
39	14	0
40	12	0
41	11	0.38
42	1	-0.38
43	11	0
44	11	-0.1
45	17	0.1
46	11	-0.1
47	17	0.1
48	11	-0.1
49	17	0.1
50	11	-0.1
51	17	0.1
52	11	-0.1
53	17	0.1

Table S7. Bond length parameters for GW409544.

Bond	Force constant	Bond Length
	10^6kJmol^{-1}nm^{-4}	nm
1 - 2	12.30	0.109
2 - 3	10.80	0.139
2 - 7	10.80	0.139
3 - 4	12.30	0.109
3 - 5	10.80	0.139
5 - 6	12.30	0.109
5 - 11	10.80	0.139
7 - 8	12.30	0.109
7 - 9	10.80	0.139
9 - 10	12.30	0.109
9 - 11	10.80	0.139

11 - 12	7.15	0.153
12 - 13	11.80	0.133
12 - 15	11.80	0.133
13 - 14	11.80	0.133
14 - 16	11.80	0.133
14 - 18	7.15	0.153
15 - 16	11.80	0.133
16 - 17	7.15	0.153
18 - 19	7.15	0.153
19 - 20	8.18	0.143
20 - 21	8.18	0.143
21 - 22	10.80	0.139
21 - 26	10.80	0.139
22 - 23	12.30	0.109
22 - 24	10.80	0.139
24 - 25	12.30	0.109
24 - 30	10.80	0.139
26 - 27	12.30	0.109
26 - 28	10.80	0.139
28 - 29	12.30	0.109
28 - 30	10.80	0.139
30 - 31	7.15	0.153
31 - 32	7.15	0.153
32 - 33	7.15	0.153
32 - 36	8.71	0.147
33 - 34	13.40	0.125
33 - 35	13.40	0.125
36 - 37	18.70	0.100
36 - 38	10.50	0.134
38 - 39	7.15	0.153
38 - 40	11.80	0.133
40 - 41	7.15	0.153
41 - 42	16.60	0.123
41 - 43	7.15	0.153
43 - 44	10.80	0.139
43 - 48	10.80	0.139
44 - 45	12.30	0.109
44 - 46	10.80	0.139
46 - 47	12.30	0.109
46 - 52	10.80	0.139
48 - 49	12.30	0.109
48 - 50	10.80	0.139
50 - 51	12.30	0.109
50 - 52	10.80	0.139
52 - 53	12.30	0.109

Table S8. Bond angle parameters for GW409544.

Angle	Force constant	Bond Angle
	$kJmol^{-1}$	degree
1 - 2 - 3	505	120
1 - 2 - 7	505	120
3 - 2 - 7	560	120
2 - 3 - 4	505	120
2 - 3 - 5	560	120
4 - 3 - 5	505	120
3 - 5 - 6	505	120
3 - 5 - 11	560	120
6 - 5 - 11	505	120
2 - 7 - 8	505	120
2 - 7 - 9	560	120
8 - 7 - 9	505	120
7 - 9 - 10	505	120
7 - 9 - 11	560	120
10 - 9 - 11	505	120
5 - 11 - 9	560	120
5 - 11 - 12	560	120
9 - 11 - 12	560	120
11 - 12 - 13	640	126
11 - 12 - 15	640	126
13 - 12 - 15	465	108
12 - 13 - 14	465	108
13 - 14 - 16	465	108
13 - 14 - 18	640	126
16 - 14 - 18	640	126
12 - 15 - 16	465	108
14 - 16 - 15	465	108
14 - 16 - 17	640	126
15 - 16 - 17	640	126
14 - 18 - 19	530	111
18 - 19 - 20	530	111
19 - 20 - 21	635	117
20 - 21 - 22	560	120
20 - 21 - 26	560	120
22 - 21 - 26	560	120
21 - 22 - 23	505	120
21 - 22 - 24	560	120
23 - 22 - 24	505	120
22 - 24 - 25	505	120
22 - 24 - 30	560	120
25 - 24 - 30	505	120
21 - 26 - 27	505	120
21 - 26 - 28	560	120
27 - 26 - 28	505	120
26 - 28 - 29	505	120
26 - 28 - 30	560	120
29 - 28 - 30	505	120
24 - 30 - 28	560	120
24 - 30 - 31	560	120
28 - 30 - 31	560	120

30 - 31 - 32	513	111
31 - 32 - 33	520	109.5
31 - 32 - 36	520	109.5
33 - 32 - 36	520	109.5
32 - 33 - 34	635	117
32 - 33 - 35	635	117
34 - 33 - 35	770	126
32 - 36 - 37	460	115
32 - 36 - 38	700	122
37 - 36 - 38	415	123
36 - 38 - 39	560	120
36 - 38 - 40	560	120
39 - 38 - 40	560	120
38 - 40 - 41	560	120
40 - 41 - 42	560	120
40 - 41 - 43	560	120
42 - 41 - 43	560	120
41 - 43 - 44	560	120
41 - 43 - 48	560	120
44 - 43 - 48	560	120
43 - 44 - 45	505	120
43 - 44 - 46	560	120
45 - 44 - 46	505	120
44 - 46 - 47	505	120
44 - 46 - 52	560	120
47 - 46 - 52	505	120
43 - 48 - 49	505	120
43 - 48 - 50	560	120
49 - 48 - 50	505	120
48 - 50 - 51	505	120
48 - 50 - 52	560	120
51 - 50 - 52	505	120
46 - 52 - 50	560	120
46 - 52 - 53	505	120
50 - 52 - 53	505	120

Table S9. Dihedral angle parameters for GW409544.

dihedral	Force constant	Phase shift	Multiplicity
	$kJmol^{-1}$		
5 - 11 - 12 - 13	16.700	-1	2
13 - 14 - 18 - 19	1.000	1	6
14 - 18 - 19 - 20	5.920	1	3
18 - 19 - 20 - 21	1.260	1	3
19 - 20 - 21 - 22	16.700	-1	2
24 - 30 - 31 - 32	1.000	1	6
30 - 31 - 32 - 33	5.920	1	3
31 - 32 - 33 - 34	1.000	1	6
31 - 32 - 36 - 38	1.000	-1	6
32 - 36 - 38 - 39	33.500	-1	2
36 - 38 - 40 - 41	33.500	-1	2
38 - 40 - 41 - 43	33.500	-1	2
40 - 41 - 43 - 44	33.500	-1	2

Table S10. Improper dihedral angle parameters for GW409544.

Improper	Force constant $kJmol^{-1}degree^{-2}$	angle degree
2 - 1 - 3 - 7	0.051	0
2 - 3 - 5 - 11	0.051	0
2 - 7 - 9 - 11	0.051	0
3 - 2 - 4 - 5	0.051	0
3 - 2 - 7 - 9	0.051	0
3 - 5 - 11 - 9	0.051	0
5 - 3 - 6 - 11	0.051	0
7 - 2 - 3 - 5	0.051	0
7 - 2 - 8 - 9	0.051	0
5 - 11 - 9 - 7	0.051	0
9 - 7 - 10 - 11	0.051	0
11 - 5 - 9 - 12	0.051	0
12 - 11 - 13 - 15	0.051	0
12 - 13 - 14 - 16	0.051	0
12 - 15 - 16 - 14	0.051	0
13 - 12 - 15 - 16	0.051	0
13 - 14 - 16 - 15	0.051	0
14 - 13 - 16 - 18	0.051	0
15 - 12 - 13 - 14	0.051	0
16 - 14 - 15 - 17	0.051	0
21 - 20 - 22 - 26	0.051	0
21 - 22 - 24 - 30	0.051	0
21 - 26 - 28 - 30	0.051	0
22 - 21 - 23 - 24	0.051	0
22 - 21 - 26 - 28	0.051	0
22 - 24 - 30 - 28	0.051	0
24 - 22 - 25 - 30	0.051	0
26 - 21 - 22 - 24	0.051	0
26 - 21 - 27 - 28	0.051	0
26 - 28 - 30 - 24	0.051	0
28 - 26 - 29 - 30	0.051	0
30 - 24 - 28 - 31	0.051	0
32 - 33 - 31 - 36	0.102	35.26439
33 - 32 - 34 - 35	0.051	0
36 - 32 - 37 - 38	0.051	0
38 - 36 - 39 - 40	0.051	0
41 - 40 - 42 - 43	0.051	0
43 - 41 - 44 - 48	0.051	0
43 - 44 - 46 - 52	0.051	0
43 - 48 - 50 - 52	0.051	0
44 - 43 - 45 - 46	0.051	0
44 - 43 - 48 - 50	0.051	0
44 - 46 - 52 - 50	0.051	0
46 - 44 - 47 - 52	0.051	0
48 - 43 - 44 - 46	0.051	0
48 - 43 - 49 - 50	0.051	0
48 - 50 - 52 - 46	0.051	0
50 - 48 - 51 - 52	0.051	0
52 - 46 - 50 - 53	0.051	0

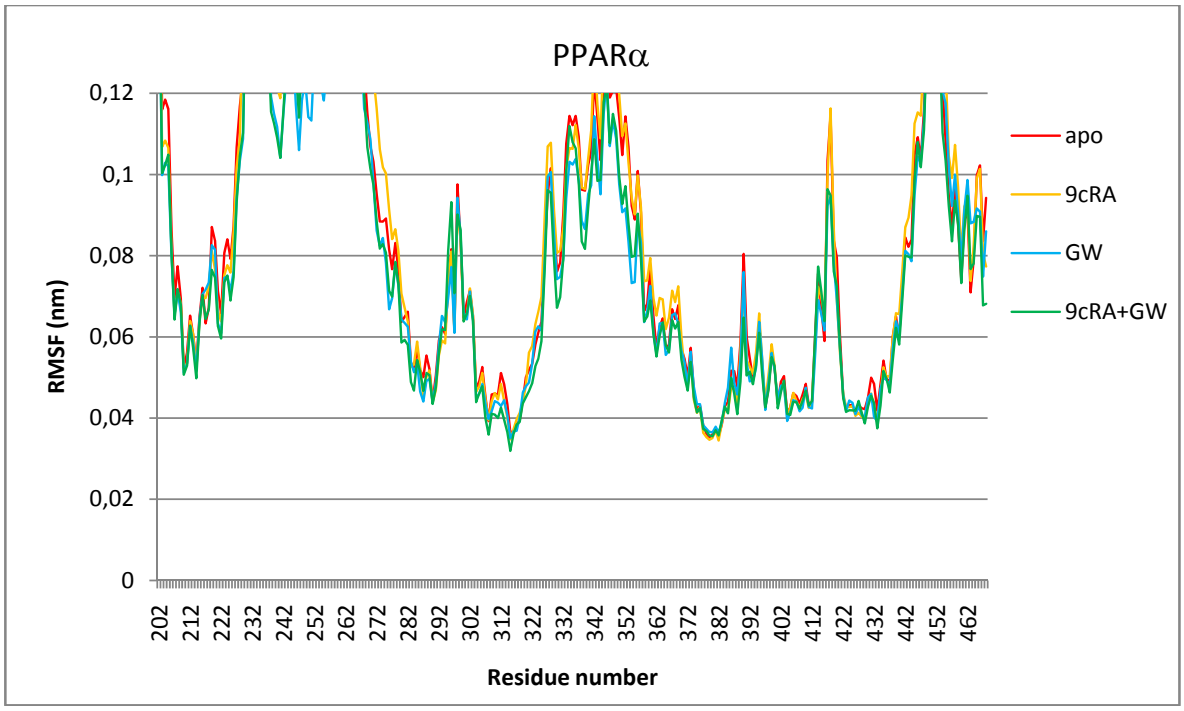

Fig. S7. Averages of RMSF values of PPARα Cα atoms in the 10 parallel PPARα-RXRα simulations.

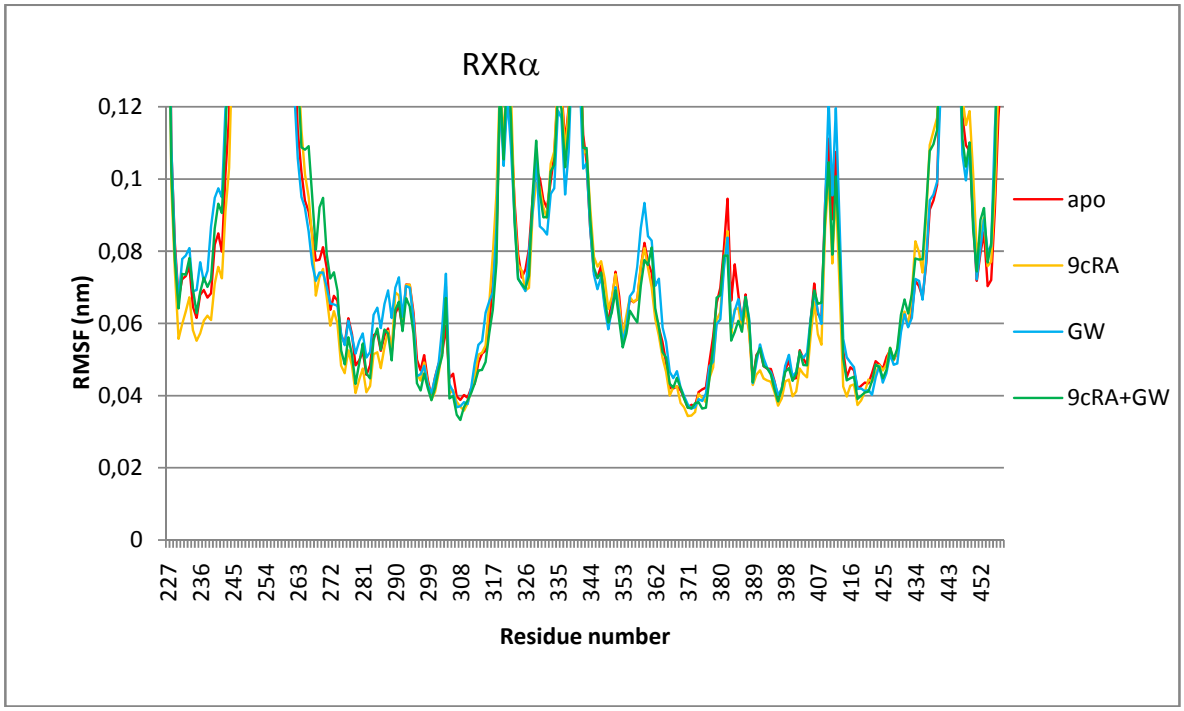

Fig. S8. Averages of RMSF values of RXRα Cα atoms in the 10 parallel PPARα-RXRα simulations.